ROYAL SOCIETY OPEN SCIENCE

royalsocietypublishing.org/journal/rsos

Research

Cite this article: Tepud-Rodríguez JS, Cotazo-Mosquera OJ, Garcia-Mora AM, Hidalgo-Troya A, Galeano L-A. 2026 Al/Co-pillaring of clays from concentrated precursors and catalytic performance in the phenol degradation by sulfate radicals. *R. Soc. Open Sci.* **13**: 251177.
https://doi.org/10.1098/rsos.251177

Received: 21 June 2025
Accepted: 30 January 2026

Subject Category:
Chemistry

Subject Areas:
materials science, environmental science, chemical engineering

Keywords:
Al/Co-pillared clay, phenol, sulfate radical degradation, heterogeneous catalysis, wastewater treatment

Author for correspondence:
Luis-Alejandro Galeano
e-mails: alejandrogaleano@udenar.edu.co; luis.alejandro.galeano@gmail.com

†Present address: Empresa de Obras Sanitarias de Pasto (EMPOPASTO S.A. E.S.P.), Carrera 24 No 21-40, Pasto, Colombia.

Supplementary material is available online at https://doi.org/10.6084/m9.figshare.c.8386439.

THE ROYAL SOCIETY PUBLISHING

Al/Co-pillaring of clays from concentrated precursors and catalytic performance in the phenol degradation by sulfate radicals

James Stith Tepud-Rodríguez[1], Omar José Cotazo-Mosquera[1], Ana Maria Garcia-Mora[1,†], Arsenio Hidalgo-Troya[2] and Luis-Alejandro Galeano[1]

[1]Grupo de Investigación en Materiales Funcionales y Catálisis (GIMFC), Departamento de Química, and [2]Grupo de Investigación Salud Pública, Departamento de Matemáticas y Estadística, Universidad de Nariño, Pasto, Nariño, Colombia

L-AG, 0000-0003-0077-2433

This study presents the first successful intercalation and pillaring of natural bentonite with mixed Al–Co species using a highly concentrated metal precursor (approx. 5.0 mol l^{-1}). A statistical design of experiments identified optimal preparation parameters for the resulting Al/Co-pillared clay (Al/Co-PILC). The clay materials were extensively characterized by atomic absorption spectroscopy (AAS), powder X-ray diffraction (XRD), N_2 adsorption–desorption, H_2-temperature programmed reduction (H_2-TPR), cationic exchange capacity (CEC), thermal analyses (TGA/DSC), and UV-vis and IR diffuse reflectance spectroscopies (DR-UV-vis and diffuse reflectance infrared Fourier transform spectroscopy (DRIFTS). The catalytic activity was assessed in the phenol degradation by sulfate radicals from sodium persulfate. The determined optimal conditions in terms of atomic metal ratio of cobalt in the interlayering solution (AMR_{Co} ~ 10 mol%) and equivalent hydrolysis ratio ($HR_{eq.}$ = 2.0) yielded a well-expanded Al/Co-PILC with basal spacing d_{001} (18.4 Å) and textural properties (S_{BET}: 194 m^2 g^{-1}; $S_{\mu p}$: 140 m^2 g^{-1}) typical of successfully pillared Al-PILCs, alongside a significantly higher amount of cobalt was effectively incorporated as compared with previous reports. This material achieved 72.0 ± 1.24% of phenol degradation and 65.0 ± 2.13% of dissolved organic carbon (DOC) removal within 1 h of reaction under circumneutral pH and ambient conditions of temperature and pressure, with negligible cobalt

leaching (approx. 0.01 mg l^{-1}). Al/Co-PILCs so prepared are thus promising active solids for catalytic advanced oxidation of biorefractory organic contaminants in highly polluted wastewater using sulfate radicals (SR-AOP).

1. Introduction

Natural clays are sedimentary rock minerals that are low cost and abundant in nature. They are made up of different types of granular and crystalline minerals, aluminosilicates and hydrated phyllosilicates [1]. The main physico-chemical and textural properties of clays depend on their morphology and degree of isomorphic substitution, which in turn determine how they are classified. Owing to its 2:1 lamellar structure, the smectic family has interesting physico-chemical properties, such as a high cationic exchange capacity (CEC), which facilitate its modification through simple chemical processes like intercalation. This makes it highly suitable for heterogeneous catalysis and adsorption [2].

To improve the catalytic and adsorption properties of these clays, different modification processes, such as impregnation and pillaring, have been studied [3]. Pillared clays (PILCs) are prepared by exchanging the cations naturally present in the clay (Ca^{2+}, Na^{+}, Mg^{2+}, etc.) for larger ones such as the Al Keggin oligocation $[AlO_4Al_{12}(OH)_{24}(OH_2)_{12}]^{7+}$, which are subsequently transformed through thermal processes into oxometallic clusters called pillars [4]. Pillars give the clay greater basal spacing, microporosity and thermal stability. Aluminium-pillared clays (Al-PILCs) have traditionally been prepared with a partially hydrolysed and highly diluted solution of Al, which, when in contact with dispersions of the clay that must be also highly diluted, allow different transition metals such as Fe, Cu, Ga, Ti or Cr [5,6] to be incorporated alongside.

The high volume required per unit of mass of the final material (approx. 3.2 l g^{-1} clay) and the long reaction time have made it difficult to prepare and use these materials on an industrial scale [3,7], as a clear barrier that has largely hindered the application of such an interesting family of sustainable and low-cost functional materials, as active solids of a variety of catalytic processes.

Recently, our group has reported the pillaring of clays from highly concentrated precursors of Al and Fe [8,9] to offset these disadvantages without significantly sacrificing the most important physico-chemical properties of Al-PILCs, even at a preparation scale of 10 kg (S_{BET} > 190 m^2 g^{-1}; $S_{\mu p}$ > 160 m^2 g^{-1}; d_{001} ~ 18.3 Å) [8]. Al/Fe-PILCs have previously performed very well in the heterogeneous Fenton degradation of organic contaminants such as dyes [10,11], phenolic compounds [12] and natural organic matter (NOM) [13,14]. However, to our knowledge, this utilitarian method of preparing PILCs mixed with Al from concentrated precursors has not yet been used to incorporate any transition metals other than iron. Although the incorporation of Co into pillared clays has been attempted previously, efforts have mainly focused on the impregnation of Co into clays previously expanded with Al or another metal of interest [15–18] to use them as adsorbents [19], Fischer–Tropsch catalysts [20–22] or in catalytic oxidation processes [23–25], where, in general, the effect of Co incorporation on the textural properties of pillared clays has been documented.

To the best of our knowledge, very few studies have looked at how clays expand with either Co or with mixed Al/Co pillars. Thomas *et al.* [26] used complex cobalt salts as pillaring agents but did not achieve the successful formation of cobalt pillars, instead obtaining clays with fragile thermal and mechanical stability. Different authors also studied the co-intercalation of smectites with mixed Al/Co polycations [19,22,24,27–29], without consistently evidencing an expansion to basal spacings greater than 17 Å or the conservation of a predominantly microporous nature, both of which are characteristic of successfully expanded Al-PILCs, nor the significant incorporation of Co in the final solids. Bertella & Pergher [30] reported so far the successful expansion of pillared clays with Al/Co (Al/Co-PILC) using diluted solutions of Al/Co hydrolysed by the conventional method with NaOH addition and a Co initial atomic ratio of 10% to 25%. However, the amounts of cobalt incorporated were lower than 0.07% w/w in the final PILCs. In the same sense, Vicente *et al.* [24] also formerly achieved Al/Co-copillaring but in the presence of saponites, a trioctahedral smectite with some significant structural differences in comparison with montmorillonites, main clay phase in natural bentonites.

On the other hand, during the past decade advanced oxidation processes based on sulfate radicals (SR-AOPs) for the decontamination of wastewater have been intensively studied, owing to the advantages of sulfate radicals ($SO_4^{\bullet-}$) over hydroxyl radicals in terms of standard reduction potential (2.5–3.1 V), longer half-life (30–40 µs) and greater selectivity towards organic compounds with unsaturated π bonds, in addition to their wider operating pH range (approx. 2.0–8.0) [31].

Sulfate radicals can be generated by heat activation, UV-vis radiation, ultrasound, pyrolysis or by catalytic activation of sodium peroxymonosulfate (PMS, HSO_5^-) or sodium persulfate (PS, $S_2O_8^{2-}$) with transition metals such as Co^{2+}, Mn^{2+}, Ce^{3+}, Ni^{2+} and Fe^{2+}. Of these methods, the Co^{n+}/PS system has demonstrated the best performance at generating sulfate radicals at neutral pH, even in the presence of very low concentrations of the oxidant precursor [32,33]. As cobalt ions dissolved in water can cause serious health problems owing to their toxicity and carcinogenicity, the catalytic activation of PMS/PS for water purification is only viable in the presence of materials that strongly immobilize the metal. Consequently, in recent years, various cobalt-based functional materials, such as cobalt oxides, spinel-type ferrites, layered double hydroxides (LDHs) and metal-organic frameworks (MOFs), have been investigated for their application in SR-AOPs [34,35]. These materials offer high redox activity and tuneable structures that favour persulfate activation. However, some exhibit drawbacks such as complex synthesis procedures, high production costs or low chemical stability of cobalt under reaction conditions, which can strongly limit their practical application. Various materials based on metal centres other than Co, such as Fe, have also shown promising results in the catalytic degradation of pharmaceuticals or dyes by using persulfate as oxidizing agent, especially by optimizing the degradation kinetics as compared with either homogeneous or heterogeneous Fenton processes. However, they display some problems common with solid Fenton catalysts, particularly a lack of good chemical stability against leaching of the active metal, decreasing the life cycle of the catalyst and its long-term efficiency [36]. The use of PS as an oxidizing agent displays some limitations, mainly when employing non-catalytic activation methods. Although PS can also generate two moles of sulfate radicals for every mole and PMS only generates one mole, in practice PMS not only generates the powerful sulfate radical but also has the capacity to directly oxidize contaminants owing to the presence of HSO_5^-, providing an additional oxidation pathway that leads to faster degradation of organics even under lower concentrations than PS (also called PDS after peroxydisulfate). However, PS has recently shown more efficient total organic carbon (TOC) removal than PMS, whereas PMS was much more effective in degradation of the antibiotic tetracycline [37].

In this context, the pillared clays emerge as an attractive alternative compared with other catalysts, since they are abundant and low-cost aluminosilicates, which can result in a reduced environmental impact, and at the same time, they can exhibit high catalytic efficiency [38]. If the efficient preparation of clays co-pillared with Al and Co can be achieved, these materials could offer a plausible way to use PMS/PS catalytic activation to purify industrial wastewater under near-neutral pH conditions.

The limited number of available studies on the incorporation of cobalt (Co) via mixed pillaring with other metals, primarily aluminium—by far the most extensively studied polycationic system—coupled with the restrictions associated with their preparation at industrial scale, including the necessity of using highly diluted precursors and the low Co content achieved in the final product, have altogether severely limited the applications of these materials, despite their high catalytic potential. Moreover, most previous works have not addressed the need for more efficient and scalable synthetic routes, leaving important research gaps that hinder their implementation in real wastewater treatment scenarios [36]. Furthermore, considering that natural clays are very low-cost materials which, when appropriately functionalized with Co, could be efficient catalysts in the degradation of persistent pollutants in wastewater, even under circumneutral pH conditions, it is interesting to explore novel preparation strategies. In this context, our work seeks to address these knowledge gaps through the application of a novel synthesis method of Al-pillared and Al/M-mixed metal pillared clays, starting from concentrated precursors, which simultaneously might allow for the incorporation of higher Co contents in the functionalized materials, thereby significantly facilitating their exploitation at industrial scale.

Consequently, the aim of this work was to optimize the preparation of co-pillared clays with aluminium and cobalt (Al/Co-PILCs) from concentrated precursors supported by statistical tools of experimental design based on three variables: (i) atomic molar ratio of Cobalt (AMR_{Co}) in the intercalating solution (10–30%); (ii) the equivalent hydrolysis ratio ($HR_{Eq.}$) in the intercalating solution (2.0–2.6); and (iii) the final calcination temperature ($T_{Cal.}$) of the modified clay (400–500°C). Physico-chemical characterization of the materials was made by conventional techniques, and their response in the catalytic activation of persulfate for the degradation of 50 mg l^{-1} of phenol (PhO) as a model biorefractory molecule was evaluated at an initial pH of 7.0, temperature of 25.0 ± 0.1°C and atmospheric pressure (76 kPa).

2. Methods

2.1. Material

The starting aluminosilicate was a low-cost Colombian calcium-rich clay, which was refined by water-dispersion followed by centrifugation to favour particle sizes smaller than 2.0 μm (hereafter referred to as AR) [39]. The clay exhibited the following chemical composition (w/w %) dry-basis: 60.25% SiO_2, 23.20% Al_2O_3, 9.37% Fe_2O_3, 3.16% MgO, 1.17% TiO_2, 0.93% CaO, 0.80% K_2O and 0.74% Na_2O, and a CEC of 143 mequiv./100 g [40].

For the preparation of the mixed Al/Co oligomeric precursors, $AlCl_3.6H_2O$ (97%, Merck®), $CoCl_2.6H_2O$ (98%, Sigma Aldrich®) and elemental aluminium (99.9% pure powder, Panreac®) were used. To determine the CEC of the clays, ammonium acetate (99.0%, Sigma Aldrich®) was employed. The catalytic experiments used phenol (99.0–100%, Sigma Aldrich®), sodium persulfate (99.0%, Sigma Aldrich®), NaOH (99.0%, Merck®), HNO_3 (65.0% Baker®), KI (99.5%, Carlo Erba®) and $NaHCO_3$ (99.7–100.3%, Panreac®), all as received. To determine the point of zero charge (pH_{PZC}), NaCl (≥99.5%, Honeywell Fluka®), NaOH (99.0%, Merck®) and HCl (37%, Panreac®) were employed. HF (40% v/v, Panreac®) and HNO_3 (65% v/v, JT Baker®) were used for the acid digestion of solid samples before atomic absorption spectroscopy (AAS) analyses.

2.2. Preparation of Al/Co-pillared clays

Aluminium/cobalt pillared clays (Al/Co-PILCs) were prepared following the methodology reported by Muñoz *et al.* [8] for the Al/Fe system, using concentrated precursors obtained through the controlled addition of metallic aluminium (Al^0). The concentrated Al/Co intercalating solutions were formulated considering the AMR_{Co} and the $HR_{Eq.}$ in the mixed Al–Co intercalating solution as experimental factors, while maintaining a constant total metal concentration (TMC) of 5.0 mol l^{-1}. In each experimental run, 10 g of refined clay (dp < 250 μm) were modified and intercalated under controlled hydrolysis and temperature conditions, followed by washing, drying and calcination at 400–500°C. The resulting materials were coded as Co_x-$Al_{y(z)}$-T, where *x*: AMR_{Co}; *y*: atomic percentage of Al; *z*: $HR_{Eq.}$, and T: temperature of calcination. In addition, a reference material was prepared by intercalating cobalt oxide onto the clay previously pillared by Al (Al-PILC), using successive cycles of exchange with Co^{2+} using a reported procedure [41]. This microencapsulated material was called CoO_x/Al-PILC. Further methodological details on the preparation of the materials are presented in the electronic supplementary material, section S1.1.

2.3. Optimization of the Al/Co-pillared clays preparation

The main preparation parameters of the Al/Co-PILC catalyst were optimized using a central composite statistical design of experiments (CCD), with a 2^3 factorial rotatable orthogonal design. This consisted of nine central points and six axial points. The factors and levels of the variables implemented in the experimental design are summarized in table 1; a more detailed rationale for the selection of each experimental response, along with its relevance to the Al/Co-pillaring optimization, is provided in the electronic supplementary material, section S1.2, table S1, whereas the specific values used in each preparation are shown in the electronic supplementary material, table S2. The full set of experiments consisted of 23 runs in a single completely randomized block. Statistical analysis of the data was performed using the response surface methodology (RSM) assisted by the Statgraphics package (Centurion XVI, v. 16.1.03). The optimization of multiple responses was carried out by constructing a desirability function, which enabled visualization of the results and the identification of the optimal catalyst preparation conditions, thereby enhancing the understanding of the process and evidence-based decision-making. The statistical significance of the variables was estimated through *p*-values less than 5%.

2.4. Physico-chemical characterization of the materials

The Al and Co contents in the solids were determined by AAS after acid digestion in a mixture of concentrated hydrofluoric and nitric acids (1 : 4 v/v). CEC was obtained by saturation with ammonium acetate and micro-Kjeldahl analysis [9]. The basal spacing of the aluminosilicates was evaluated by

Table 1. Factors and levels used in the statistical design of experiments to optimize the preparation of Al/Co-PILCs.

experimental variables	units	low level	high level
atomic metal ratio of cobalt (AMR_{Co})	Co w/w %	10.0	30.0
equivalent hydrolysis ratio ($HR_{Eq.}$)	mol OH^-/mol metal	2.0	2.6
calcination temperature ($T_{cal.}$)	°C	400	500

powder X-ray diffraction (XRD), while their porous structure and surface were determined from N_2 adsorption–desorption isotherms at 77 K using the Brunauer–Emmett–Teller (BET) method and *t*-plot analysis [8]. Thermal changes in the materials were studied using simultaneous thermal analysis (TGA/DSC). Selected materials were also analysed using hydrogen temperature-programmed reduction (H_2-TPR). Besides, UV-vis spectra were recorded to identify the transition metal coordination environment, whereas diffuse reflectance infrared Fourier transform spectroscopy (DRIFTS) spectra were used to identify surface species. The pH at the zero-charge point was determined by titration [42]. The full instrumental conditions and detailed procedures for each technique are described in the electronic supplementary material, section S1.3.

2.5. Catalytic experiments

The catalytic response of each of the materials was considered to help optimizing the Al/Co-PILC preparation method. To do this, 50 mg l^{-1} of phenol (38.3 mg l^{-1} of dissolved organic carbon (DOC)) was oxidized in the presence of PS in an aqueous system. The tests were carried out in a 1.5 l semi-batch reactor stirred at 400 r.p.m., equipped with a jacket connected to a thermostatic bath for temperature control, and a peristaltic pump to feed the reactor with a PS solution under constant flow and atmospheric pressure (76 kPa). The amount of catalyst supplied to the reactor was calculated by considering the experimentally measured cobalt content in each material and the constant doses of 0.005 mg Co/mg PS and 35.0 mg PS/mg DOC. The reactor was initially loaded with 0.5 l of the phenol solution and the Al/Co-PILC catalyst. During the first 30 min, stabilization between the solid phase and the liquid phase was permitted and the reaction pH was adjusted to a value of 7.0 using drops of NaOH or HNO_3 (0.1 mol l^{-1}), but this was not controlled during the rest of the reaction. After 30 min, 100 ml of PS (21.2 mmol l^{-1}) were gradually added under a flow of 1.67 ml min^{-1} for 60 min to keep the total reaction volume as constant as possible and avoid dilution inside the reactor during sampling. Zero reaction time was established as the time when the PS solution was first added. Twenty-five millilitres of the sample were taken every 15 min during the reaction time. The total time recorded for each experiment was 120 min (30 min of pre-stabilization, 60 min of PS addition and 30 min of post-treatment). Each sample was microfiltered (Millipore®, 0.45 µm) to separate the suspended catalyst before analysing the PS concentration, the removal of DOC and the phenol concentration by high performance liquid chromatography (HPLC). Additionally, to evaluate the chemical stability of the Al/Co-PILC catalyst in the degradation of phenol, the reusability of the catalyst was assessed over five consecutive catalytic cycles, after which the catalyst was filtered, recovered and washed multiple times with UHP water. The recovered catalyst at the end of the cycles was characterized, and the amount of dissolved metal ions (Al and Co) in each reaction's effluent was monitored using AAS.

2.6. Analytical methods

The response parameters evaluated in the catalytic assays were: (i) the percentage of PS consumed, determined by the iodometric method as described by Liang *et al.* [43]; (ii) phenol degradation, quantified by HPLC/photodiode array (PDA) using a C_{18} column and a gradient elution; and (iii) the decrease in the DOC content, measured as an indicator of the degree of the carbon mineralization. At the end of each assay, the catalyst was recovered by filtration, and its chemical stability was indirectly verified by AAS, analysing the concentrations of Co and Al released into the effluent of reaction. The reliability of the results was ensured by updated calibration curves and repeatability controls for PS, phenol and DOC measurements. Detailed experimental conditions and complete analytical procedures are described in the electronic supplementary material, section S1.4, and a graphical description of the quality controls, calibration and methodological validation is presented in the electronic supplementary material, section S2, figures S8–S14.

3. Results and discussion

3.1. Statistical analysis of Al/Co-pillaring from concentrated precursors

The statistical design of experiments used the atomic ratio of cobalt in the intercalant solution (AMR_{Co}), the equivalent hydrolysis ratio ($HR_{Eq.}$) and the final calcination temperature of the clay ($T_{Cal.}$) as experimental factors. The effect of these factors on the physico-chemical properties and the catalytic response of Al/Co-PILCs in the degradation of phenol (PhO) by sulfate radicals was studied by running the set of experiments presented in the electronic supplementary material, table S2. Individual analysis of each of the responses was then carried out using the RSM, analysis of variance (ANOVA) and multi-response optimization based on the desirability function. The complete results are summarized in table 2. The analysis of variance (electronic supplementary material, table S3) shows that experimental factor AMR_{Co} affected the responses with the greatest statistical significance, especially those that govern the structural expansion of the aluminosilicate (d_{001}, full width at half maximum (*fwhm*)). The incorporation of cobalt ($Co_{inc.}$), on which the catalytic response of the solids largely depends, also had a significant effect, as well as the electrical conductivity (EC) of the intercalating solutions, which will be discussed in detail later. On the other hand, as expected, the $HR_{Eq.}$ factor exerted a statistically significant first-order effect on the final pH of the hydrolysed Al/Co oligomeric precursor, and a second-order effect on EC, the final density of the solutions (ρ) and the phenol degradation. The final $T_{Cal.}$ of the solids did not significantly affect any of the responses studied, although it did affect some physico-chemical properties that were not incorporated into the statistical models, as discussed later.

After disregarding statistically insignificant values of the terms, the results were fitted to quadratic statistical models for each individual response (electronic supplementary material, scheme S1). Positive and negative coefficients indicate terms that positively or negatively affect the response, respectively [44–46]. The coefficient of determination (R^2) allowed the level of adjustment of each response to be estimated as a function of the experimental factors (electronic supplementary material, table S3). The values taken were 53% to 84%, which are satisfactory for the expressed quadratic models (electronic supplementary material, equations (S2–S10), scheme S1).

3.2. Physico-chemical characteristics of the materials

The physico-chemical characteristics of the hydrolysed Al/Co solutions are summarized in table 2. The solutions prepared using the concentrated precursor methodology, including those with high $HR_{Eq.}$ values, did not contain any precipitated species or suspended solids despite the high concentration of metals used (TMC ~ 5.0 mol l^{-1}). This shows that Al/Co system is stable under elevated metal concentrations as high as those here employed. On the other hand, the intercalating solutions presented high EC values (95–120 mS cm^{-1}) compared with those reported for systems such as Al/Fe at similar concentrations (approx. 60 mS cm^{-1}) [8,9]. The decrease in EC with hydrolysis allows the degree of oligomerization that metals undergo to be indirectly monitored, owing to the decrease of the positive charge per metal atom (+0.54) since Keggin-type polycations are formed with the tentative formula $(Al_{13-x}Co_x)^{7+}$. It can therefore be deduced that the isomorphic substitution of cobalt atoms in polynuclear Al species is more difficult than substitution with Fe atoms. The electrical conductivity of aqueous solutions of Co^{2+} at a pH close to 3.0 is only slightly higher than the one of Fe^{2+}. Consequently, the differences measured in the Al^{3+}-mixed intercalant solutionscannot be attributed to either significant differences in ionic size, solvation or the charge of the two transition ions in the range of final pH values exhibited by the hydrolysed solutions (table 2). This was also verified by the fact that the fraction of Co in the intercalating solutions displayed a statistically significant effect on the final EC (electronic supplementary material, table S3).

On the other hand, an increase in final pH was observed in all the solutions as the hydrolysis progressed and this was in proportion to the $HR_{Eq.}$. Such behaviour is consistent with a higher concentration of hydroxide ions resulting from the dissolution of a higher fraction of Al^0. It is worth mentioning that the controlled use of metallic Al^0 as a precursor in our high-concentration metal hydrolysis system not only allows for the gradual and *in situ* release of hydroxide ions (OH^-), but also facilitates the progressive hydrolysis of Al^{3+} and Co^{2+}. This hydrolysis favours the generation of oligomerized polynuclear species with a high positive charge, such as Keggin-type species (Al_{13}^{7+} and $(Al_{13-x}Co_x)^{7+}$). These polycationic species are primarily responsible for initially expanding the starting aluminosilicate, and after the heat treatment, they provide stability and homogeneous distribution of

Table 2. Physico-chemical and catalytic features of the interlayering solutions and the Al/Co-modified clays. EC: electrical conductivity of intercalant solution; ρ: density of the intercalant solution; S_{BET}: BET specific surface area; $S_{\mu p}$: microporous surface area.

Sample	EC (mS cm^{-1})	ρ (g ml^{-1})	Co$_{inc.}$[a] (w/w %)	d_{001}[b] (Å)	pH$_i$[c]	pH$_f$[c]	*fwhm*[b] (°2 θ)	S_{BET} (m^2 g^{-1})	$S_{\mu p}$ (m^2 g^{-1})	PhO degrad.[d] (%)	Co leaching (mg l^{-1})
AR	NA	NA	NA	14.1	NA	NA	1.61	79	33	9	NA
$Co_{10}Al_{90}$ (2)-400	109.6	1.157	0.404	18.4	−0.74	2.25	1.38	195	140	72	0.011
$Co_{10}Al_{90}$ (2)-500	109.1	1.154	0.349	17.4	1.96	2.29	1.14	177	134	70	0.012
$Co_{10}Al_{90}$ (2.6)-400	106.3	1.102	0.375	15.9	1.88	3.24	1.57	161	132	57	0.038
$Co_{10}Al_{90}$ (2.6)-500	108.5	1.070	0.300	14.0	1.91	3.12	1.45	132	98	38	0.026
$Co_{20.40}Al_{80}$ (1.8)-450	94.2	1.138	0.358	14.3	1.84	2.80	1.35	142	96	52	0.011
$Co_{20}Al_{80}$ (2.3)-450*	118.3	1.191	0.363	15.2	1.80	2.67	1.41	162	122	38	0.038
$Co_{20}Al_{80}$ (2.8)-450	100.3	1.113	0.335	13.8	2.34	3.33	1.47	124	75	55	0.015
$Co_{20}Al_{80}$ (2.3)-365.9	117.2	1.245	0.427	13.8	1.98	2.62	1.28	146	103	63	0.027
$Co_{20}Al_{80}$ (2.3)-534.1	112.9	1.190	0.347	13.9	1.85	2.35	1.47	157	112	55	0.049
$Co_{30}Al_{70}$ (2)-400	108.3	1.133	0.491	9.83	0.98	2.95	1.87	118	87	48	0.036
$Co_{30}Al_{70}$ (2)-500	106.7	1.145	0.410	9.86	1.94	2.92	1.97	106	74	21	0.025
$Co_{30}Al_{70}$ (2.6)-400	113.3	1.150	0.442	10.1	2.64	3.15	1.85	103	86	43	0.023
$Co_{30}Al_{70}$ (2.6)-500	115.8	1.158	0.399	10.1	2.58	3.17	1.86	97	67	37	0.022
$Co_{3.18}Al_{97.8}$ (2.3)-450	98.7	1.135	0.079	13.3	−0.42	2.88	1.68	87	39	21	0.026
$Co_{36.8}Al_{63.2}$ (2.3)-450	136.5	1.179	0.602	9.92	2.34	2.76	1.95	138	82	32	0.032
CoOx/Al-PILC	50.2	1.082	2.841	16.8	1.82	3.52	1.69	139	55	71	0.103

*Average of the nine central points of the statistical design of experiments.

[a]Determined by AAS on the solid materials.

[b]Full width at half maximum determined by XRD on the powder samples.

[c]pH$_i$/pH$_f$ refers to the pH of the intercalating solutions at the beginning and at the end of the hydrolysis process, respectively.

[d]Determined by HPLC for each sample after 120 min of testing.

the pillars within the interlayer microporous network [8]. Finally, hydrolysis through the dissolution of Al^0 showed the advantage of producing hydrogen, which, when recirculated, can be used to heat the reaction system itself, thus increasing the sustainability of the material's preparation procedure.

It is worth noting that as the atomic fraction of Co in the solutions increased, the pH_f also increased. However, at a constant $HR_{Eq.}$, the pH_i values also increased, and in all cases the final pH values were below the optimal range reported for the formation of Al Keggin-type polyoxocations (pH: 3.5–4.5) [10,47]. According to Muñoz *et al.* [8], for the Al/Fe system in a concentrated medium, low values of final pH can indicate a very rapid reaction of OH^- ions, generating species with both large size and high charge, even in early stages of basic hydrolysis, owing to a wider distribution of polycationic metal species. However, this does not seem plausible for the Al/Co system, since the atomic fraction of Co did not exert a statistically significant effect on the final pH of the intercalating solutions (electronic supplementary material, table S3), possibly because the Co in solution is not as unstable as Fe upon increasing pH. There was also no significant change in the density of the intercalating solutions because of any of the three factors evaluated in this research, which suggests that this variable mostly depends on the TMC value used for the preparation of the intercalating solutions, which was constant in all experiments here reported. In the following sections, correlation will be made between the experimental factors evaluated in this study and the possible formation of mixed Al/Co polyoxocations in the hydrolysed solutions.

The physico-chemical characteristics of the Al/Co-PILCs are summarized in table 2 and the electronic supplementary material, table S4. First of all, figure 1 shows that the starting clay exhibits a d_{001} signal at approximately 6.3° 2θ, characteristic of a predominantly calcium montmorillonite phase (JCPDS 00-003-0010), with a possible minor mixture of a sodium phase (JCPDS 00-012-0232). The material preserved this signal in all cases, demonstrating that it has not been either delamined or collapsed by the heating between 400 and 500°C. These basal d_{001} spacings determined by XRD decreased markedly with an increasing AMR_{Co} in the intercalating solutions (figure 1 versus the electronic supplementary material, figure S1). This was also statistically validated by the analysis of variance (electronic supplementary material, table S3). Clays modified with up to 20% Co (electronic supplementary material, figure S1) consistently yielded basal spacings higher than that of the starting material (AR, d_{001} = 14.11 Å). However, only samples prepared with 10% Co showed a significant and clearly differentiated increase in d_{001} reaching a maximum of 18.4 Å ($Co_{10}Al_{90}$(2)-400). This shift of d_{001} suggests that the intercalating solutions prepared with 10% Co presented a greater degree of metal condensation in the form of Keggin-type polyoxocations, compared with those prepared with a higher percentage of Co, thus facilitating the formation of the Al/Co pillars after the final calcination process. Additionally, the *fwhm* values for the materials prepared with 10% Co were between 1.14 and 1.57° 2θ, revealing a more uniform distribution of molecular sizes in the intercalated polycations [8].

It is worth noting that in the present study, the Co content incorporated in Al/Co-PILCs prepared with 10% AMR_{Co} from concentrated precursors (0.404% w/w) was almost 40 times higher than that previously reported (approx. 0.010% w/w), and about 6 times higher than that reported in the presence of 25% Co (approx. 0.069% w/w) [30], in both cases using diluted precursors. This is important because it highlights the advantages of using concentrated precursors in the preparation of Al/Co-PILCs, where the increase in TMC allowed for a notable rise in the incorporation of Co into the pillared clay, without sacrificing the structural expansion or the textural properties characteristic of Al-PILCs. Besides, there is a significant reduction in the working volume per unit mass of the final prepared material, in a factor close to 100 times lower, as previously reported in the preparation of Al/Fe-PILCs [8], which is essential in order to successfully scale-up the preparation of this family of functional materials.

On the other hand, samples prepared with atomic fractions greater than 10% Co generally showed a decrease in d_{001} and in some cases values even lower than that of the starting clay (electronic supplementary material, figure S1). This suggests that such solutions experienced a lower degree of oligomerization of the metals towards intercalating polycations, giving rise to only incipiently pillared clays at best [10,48]. The percentages of compensated CEC remained similar up to an AMR_{Co} of 20% but decreased drastically in the materials modified with solutions of 30% of Co or more. Meanwhile, the *fwhm* values (approx. 1.95° 2θ) evolved with the same trend but in the opposite direction, suggesting poor cationic compensation and a much broader distribution of interlayer spacings of the clay as a function of AMR_{Co}. In fact, the clays modified with 30% Co showed d_{001} values close to those reported for completely collapsed smectites (d_{001} ~ 9.96 Å), corresponding to the typical thickness of the 2 : 1 structure of these clays [9,30]. On the other hand, the CoO_x/Al-PILC reference microencapsulated material presented a shift in d_{001} from 17.7 to 16.8 Å (electronic supplementary material, figure S2) after the incorporation of cobalt (approx. 2.84% w/w), suggesting that, despite the higher percentage

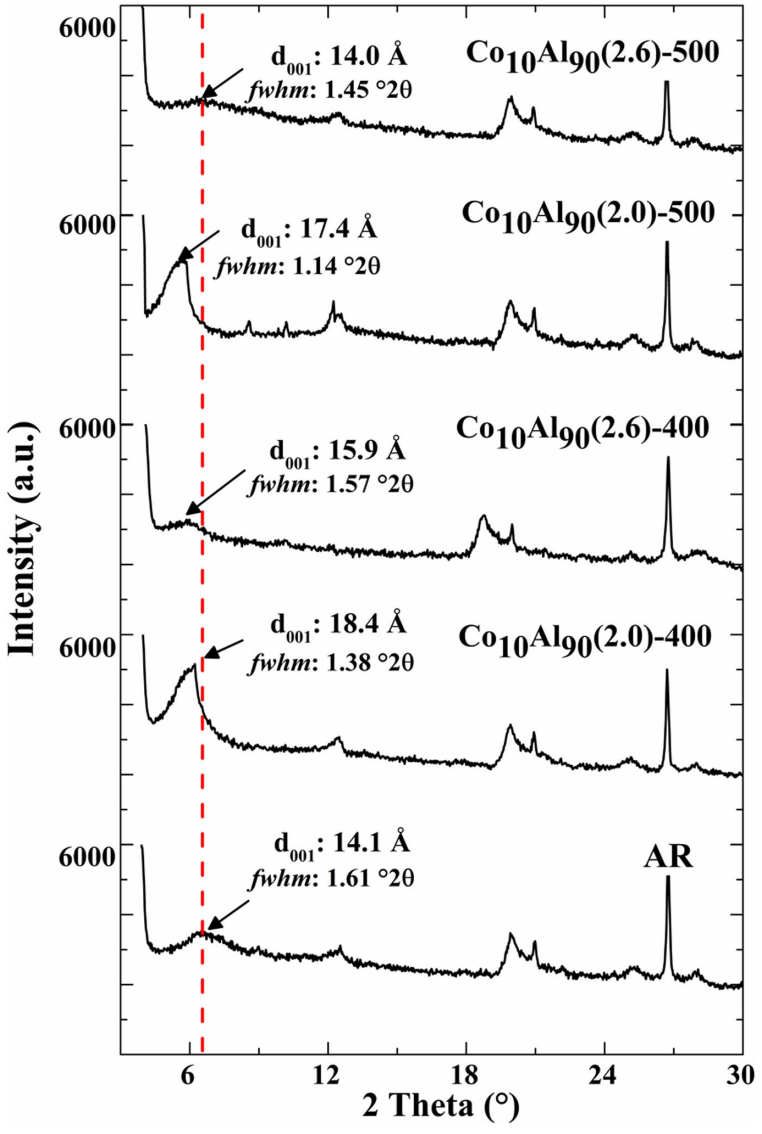

Figure 1. Powder XRD patterns for the starting refined clay (AR) and 10% Co modified clays.

of cobalt incorporated into the final solid, both the basal spacing and the distribution of species got deteriorated (*fwhm*: 1.69° 2θ). It probably arose on the acid properties of the intercalated Co ions [41].

Figure 2 and the electronic supplementary material, figure S3 show the N_2 adsorption/desorption isotherms of the starting material and selected Al/Co-modified materials. The isotherms of the modified materials were type IV according to IUPAC [49], which are characteristic of solids exhibiting both mesoporosity and microporosity [50]. Furthermore, the long and narrow H3-type hysteresis indicates the existence of narrow mesopores [49], typical of lamellar aggregates where the particles form slit-shaped pores [9]. This also demonstrates that the lamellar structure of the clay was preserved and was not affected by the pillaring process [8]. Therefore, the increase in the adsorbent capacity of the Al/Co-PILCs with respect to the starting material must correspond to the formation of mesoporosity and microporosity because of the intercalation process. In general, the textural properties of the modified materials (table 2) showed a significant increase in the BET surface area (up to 195 $m^2\ g^{-1}$, of which $S_{\mu p}$: 140 $m^2\ g^{-1}$, with average pore widths of approximately 4.8 Å) as compared with the AR starting material (S_{BET}: 79 $m^2\ g^{-1}$; $S_{\mu p}$: 33 $m^2\ g^{-1}$). It is evident that the increase in both the BET surface and the microporosity content of the modified materials was inversely proportional against both the fraction of Co in the intercalating solutions (mainly for AMR_{Co} > 20%) and the calcination temperature under constant hydrolysis ratio. The surface increase for the materials modified with 20% AMR_{Co} was not accompanied by the basal spacings characteristic of pillared clays. In other words, the textural data therefore suggest that for these samples a fraction of the cobalt was incorporated directly onto the surface of the clay or in its interlayer, increasing S_{BET} but not necessarily $S_{\mu p}$, thanks

to the possible incorporation of Co oxides within the pores of the starting material [15,23]. In the CoO_x/Al-PILC reference microencapsulated material, the incorporation of cobalt strongly decreased $S_{\mu p}$, previously achieved thanks to the Al-pillaring, from 103 to 55 $m^2\ g^{-1}$, suggesting that the metal oxide particles partially blocked the microporosity. Therefore, the strong correlation between the increase in the textural properties and the d_{001} basal spacing in the materials modified with 10% Co, supports the predominant intercalation of mixed Al/Co pillars in the clay interlayer of these materials, as formerly suggested by other authors [30,48]. The formation of mixed Al/Co pillars depends on the ability of Co^{n+} to isomorphously substitute Al^{3+} ions in the Keggin-type polycation during hydrolysis. Previous works on the intercalation of clays with mixed Al/M pillars [10,51] have shown that the increase in the fraction of M in the intercalating solutions does not necessarily promote a higher proportion of this metal in the intercalated polycations, and therefore, they are not stabilized in the final Al/M-PILCs. This is mainly influenced by the acid/base characteristics of M, the pH of the intercalating solution, the total concentration of metals and, primarily, the similarity between its ionic radius and that of Al^{3+}. Therefore, the samples intercalated with 10% Co suggest that mixed Al/Co pillars were stabilized owing to the increase in the basal spacing of the aluminosilicate to values comparable to those of Al-PILCs, which is a result of the partial isomorphic substitution of Al^{3+} for Co^{2+}. Although the ionic radii of both Co^{n+} and Fe^{n+} ($2^+/3^+$) are somewhat far from that of Al^{3+} (approx. 53 pm O_h, approx. 67.5 pm T_d), the incorporation of Co into clays through hydrolysed Al/Co solutions is probably more restricted than that of Fe with Al/Fe solutions [10,28]. This is because at pH conditions close to 3.0, at which this type of hydrolysed solution is stabilized in the two bimetallic systems, iron is stabilized predominantly as Fe^{3+} (approx. 63 pm in a tetrahedral environment, and approx. 78 pm in an octahedral environment). By contrast, cobalt is almost completely restricted to its Co^{2+} state (approx. 72 pm in a tetrahedral environment, and approx. 74 pm in an octahedral environment). This finding is further corroborated by the analysis of the absorption bands in the DR-UV-vis spectra (figure 3), whose signals at 208 and 272 nm are attributed to Co–Al interactions associated with Co^{2+} atoms coordinated with the aluminosilicates in tetrahedral positions. These were followed by a signal near 430 nm possibly related to the coordination of Co^{2+} in octahedral positions. However, as this signal is wide, it may also correspond to Co^{3+} ions in octahedral positions overlapping the signal of the Co^{2+} species mentioned above [52–54]. Therefore, for both transition metals, the structural sites of the Keggin polycation with an Al(IV) tetrahedral environment seem to be where the isomorphic substitution of Al^{3+} can occur most easily. As these sites are also the scarcest in the oligocation, it would explain the low percentages of incorporated metals. It has been reported that in alumina impregnated with Co, octahedral Co^{3+} is more stable than octahedral Al^{3+}, thereby facilitating the replacement of octahedral Al^{3+} with Co^{3+} in spinel-type mixed oxides [30,55]. However, the substitution of Co^{2+} is more limited than that of Fe^{3+} in hydrolysed Al oligocations.

The $HR_{Eq.}$ and $T_{Cal.}$ of the solids prepared with 10% Co also affected the physico-chemical characteristics of the final materials. In general, at higher values of $HR_{Eq.}$ and $T_{Cal.}$, the d_{001} decreased and the *fwhm* increased, suggesting that polyoxocations in the intercalating solutions exhibited a higher degree of metal oligomerization and a narrower molecular size distribution for $HR_{Eq.}$ values close to 2.0 and calcination temperatures closer to 400°C. Such results are consistent with those reported by Bertella & Pergher [30], who stated that a hydrolysis ratio of 2.0 and a $T_{Cal.}$ of 450°C were the best conditions to prepare Al/Co-PILCs, in their case from a diluted oligomeric precursor.

The hydrogen temperature programmed reduction (H_2-TPR) patterns of the starting material and selected Al/Co-PILCs are compared in figure 4. The AR starting clay showed events mainly associated with the reduction of both extra- and structural iron oxides of the aluminosilicate, discussed in detail in previous studies [10,40], briefly as follows: (i) the reduction of extra-structural iron oxides is attributed to sequential steps ($Fe_2O_3 \rightarrow Fe_3O_4$; T_{M1} = 575°C), (ii) the reduction of iron oxides under strong interaction with Al_2O_3 ($T_{M2} \sim 650$°C) is owing to the reduction of magnetite to wüstite ($Fe_3O_4 \rightarrow FeO$), and (iii) the reduction of iron in the structural sheets of the clay is naturally less accessible, leading to higher temperatures ($T_{M3} \sim 800$°C) ($Fe_2O_3 \rightarrow Fe^0$). Accurate assigning of reduction events is difficult for both alumina and aluminosilicates modified with cobalt owing to the complex interactions undergone by cobalt oxides with aluminosilicates. However, the materials increased the consumption of H_2 irrespective the changes in the preparation parameters, alongside the shift of some AR reduction events towards lower temperatures after intercalation/pillaring. The first reduction signal at approximately 490°C can be attributed to the presence of easily accessible extra-structural cobalt oxides on the aluminosilicate surface without strong interaction ($Co_3O_4 \rightarrow CoO \rightarrow Co^0$) and whose complete reduction has been reported to take place between 300 and 580°C [56,57]. However, a previous study on the same type of clay found that the extra-structural iron oxides

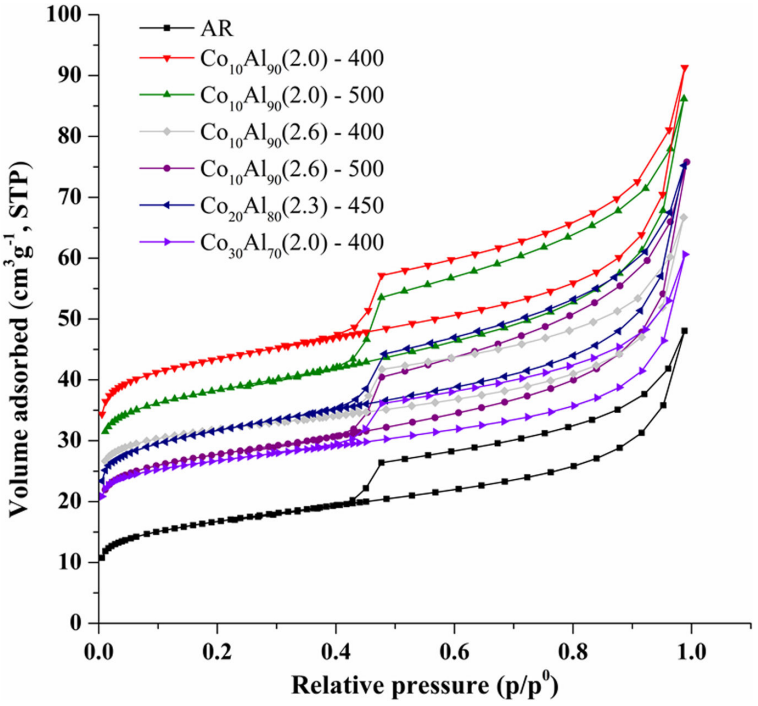

Figure 2. N_2 adsorption/desorption isotherms of Al/Co-PILC materials prepared with 10% to 30% Co.

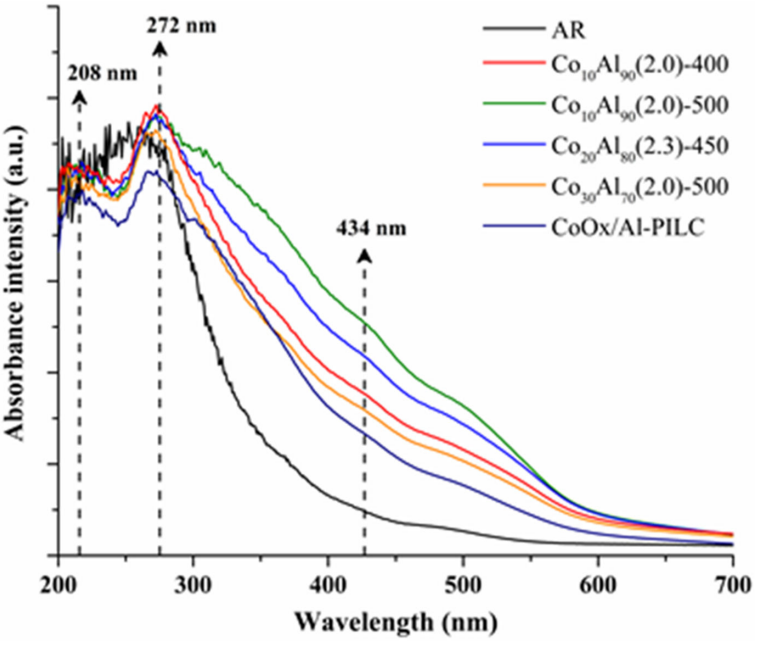

Figure 3. DR-UV-vis spectra of cobalt-modified materials and the AR refined clay.

that were originally part of the starting clay got more exposed owing to the structural expansion of the clay, leading this signal to appear at a lower range of temperatures, almost identical to that observed in the present study [40]. Taking it into account, and the relatively low Co content in the modified materials as compared with the iron content in AR, the second explanation seems much more plausible. A second and even third reduction event appeared between 590 and 620°C in the pillared materials (AMR_{Co} = 10%), which can be associated with the reduction of Co-sites more strongly interacting with Al in weakly linked particles deposited on the aluminosilicate's surface. However, considering the low recorded hydrogen consumption (less than 80.0 µmol g^{-1}), they do not seem to have been formed significantly in these materials, still more considering that AR also exhibited a small shoulder in the same region (647 °C) [20,25,58]. A fourth event can be seen between 800 and 820°C

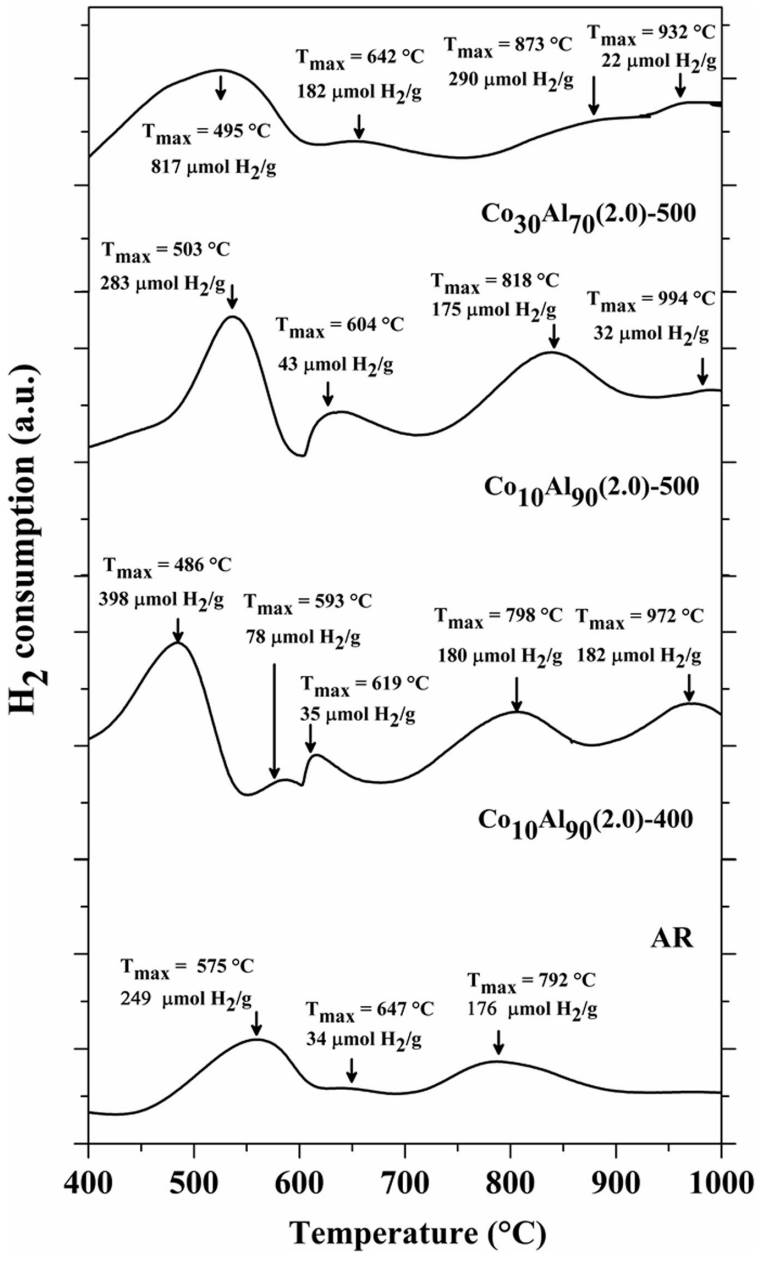

Figure 4. Temperature programmed reduction profiles (H_2-TPR) for the starting refined clay (AR) and selected Al/Co-PILCs.

that can be entirely attributed to the starting clay, with a hydrogen consumption almost identical, and the reduction temperature only slightly shifted towards a higher value as compared with that observed in AR (792°C). Finally, it should be noted that only the pillared materials showed a final reduction event at very high temperatures, close to 1000°C. This thermal event could be attributed to the reduction of either cobalt ions being part of truly mixed Al/Co pillars, analogous to what was previously discussed for the Al/Fe-PILC system [10], or within an Al–Co spinel phase strongly linked to the aluminosilicate, which, according to different investigations, may be generated by the interaction of cobalt with Al_2O_3 supports; this may resemble the contents of mixed SiO_2 and Al_2O_3 oxides present in the tetrahedral layers of the clay [18,24,53,57,59]. It is worth noting that the signal at such high temperatures only revealed significant hydrogen consumption for the two correctly pillared materials. By contrast, although the $Co_{30}Al_{70}$(2.0)-500 material, which exhibits a basal spacing consistent to the collapsed aluminosilicate, shows a signal at 932°C, it does not have a hydrogen consumption comparable to that of the two samples modified with 10% Co. In this sample, the increase in H_2 consumption for the first thermal event was clearly more noticeable, being more than double that recorded in the pillared materials. Despite tripling the fraction of Co in the intercalating solution (AMR_{Co} = 30), the resulting material did not display a noticeable increase in the percentage of incorporated metal (table

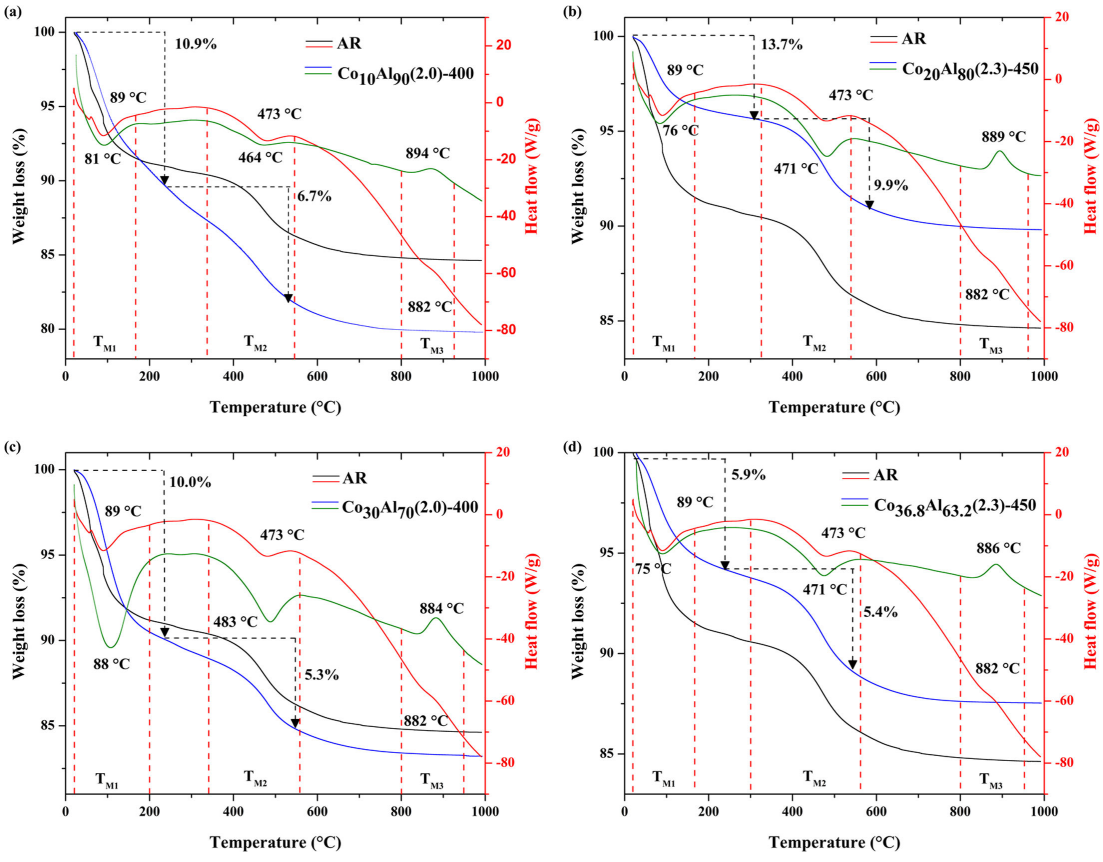

Figure 5. TGA/DSC thermal diagrams for the starting refined clay (AR) and selected Al/Co-PILCs: (a) $Co_{10}Al_{90}$(2.0)-400; (b) $Co_{20}Al_{80}$(2.3)-450; (c) $Co_{30}Al_{70}$(2.0)-400 and (d) $Co_{36.8}Al_{63.2}$(2.3)-450.

2); rather than efficiently expanding the structure, it collapsed it, while hydrogen consumption shifted mainly towards the lower reduction temperature (figure 4). This suggests that the Co species in this material were mostly stabilized through oxide particles on the surface, while the formation of Al/Co intercalating polycations that could structurally expand the aluminosilicate was rather inhibited.

The analysis of the materials by H_2-TPR has proven particularly useful for assessing the accessibility of the metallic species stabilized within the obtained solids, as well as their degree of interaction with the structural sheets of the starting aluminosilicate. Scanning electron microscopy with energy-dispersive X-ray spectroscopy (SEM-EDS) has been used previously to characterize the morphology of Al/Fe-PILCs [8,10], demonstrating a uniform distribution of the incorporated metals when the predominant formation of mixed pillars is ensured, as in the case of samples properly pillared in this work. Therefore, given the similarity between the preparation conditions reported for the Al/Fe-PILCs with those used in this work, alongside the low Co loading in the final solids, it can be inferred that the cobalt active sites in the well-pillared samples, especially in the case of $Co_{10}Al_{90}$(2)-400 and $Co_{10}Al_{90}$(2)-500, were both stabilized and homogeneously distributed throughout the microporous architecture provided by the expanded interlayer space of the pillared aluminosilicate.

Figure 5 compares the TGA/DSC thermograms for the AR clay and some representative solids (the CoO_x/Al-PILC reference microencapsulated material in the electronic supplementary material, figure S4), as well as the temperatures and weight changes seen in all the materials prepared in the electronic supplementary material, table S4. Firstly, it can be observed that the modified samples generally anticipated the first thermal event to lower values of temperature (T_{M1}), which can be attributed to a greater adsorbent's capacity; the weight percentage associated with the thermal event also increased. The same trend was observed in the second thermal event (T_{M2}), with the difference that in some cases the temperature even increased for the highest Co fractions in the intercalating solution when compared with that exhibited by AR. It is worth noting that the decrease in the maximum temperature of the second thermal event (T_{M2}) correlated well with the improvement in the textural properties and the increase in the d_{001} basal spacing of the materials (table 2). This may be because the second thermal event corresponds to the condensation and release of water molecules resulting from the

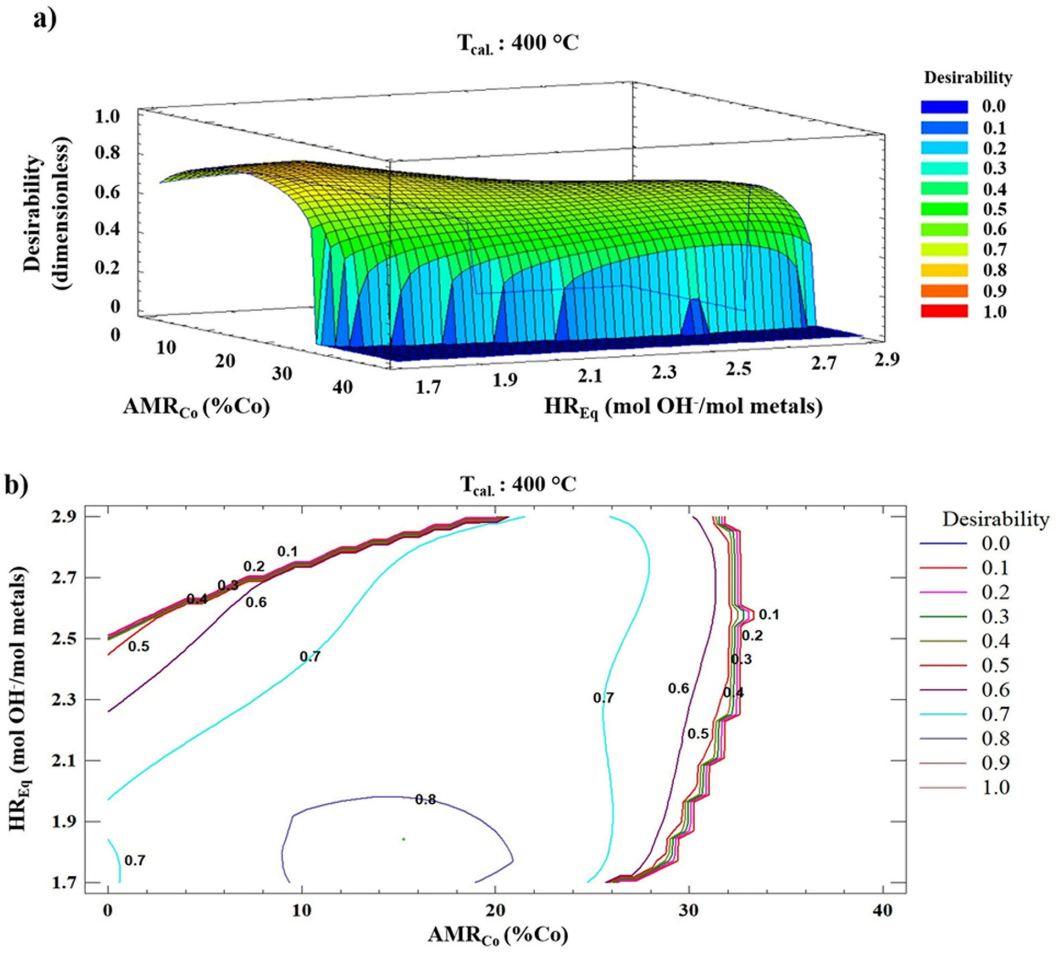

Figure 6. Multi-response analysis for the statistical design of experiments: (a) response surface estimated by the desirability function; (b) contour diagram.

structural dehydroxylation of the OH^- groups in the octahedral layers of the aluminosilicate, which clearly occurred at a lower temperature, allowing the aluminosilicate to expand more efficiently via intercalation/pillaring [10]. All samples also exhibited an exothermic event (T_{M3}) (approx. 900°C, electronic supplementary material, table S4) corresponding to a phase transition caused by losing the lamellar stacking pattern of the clay, but whose maximum temperature did not correlate with the structural expansion or textural properties of the final material. Finally, the DRIFTS spectra of the starting material and some modified materials (electronic supplementary material, figures S5 and S6) show that altering the materials using concentrated precursors did not impact the lamellar structure of the clay. This agrees with what was observed in the thermal analyses, regardless of whether pillaring of the aluminosilicate was successful [24,60–63].

3.3. Multi-response statistical optimization for the preparation of Al/Co-pillared clays as catalysts for the degradation of phenol at circumneutral pH by sulfate radicals

The multi-response surface and contour plots are presented in figure 6. The simultaneous optimization of multiple responses was carried out using the desirability function constructed through the set of modelled optimal for each of the individual responses (electronic supplementary material, scheme S1). The maximum desirability obtained was 0.83 on a scale from 0.0 to 1.0, with a slight increase in curvature towards low values of AMR_{Co} and $HR_{Eq.}$ and a $T_{Cal.}$ of 400°C, which means that at least 83% of the combination of responses considered can be predicted by the statistical model. This level of adjustment is very acceptable, especially considering that such a high number of responses considered simultaneously could lead to greater variability in fulfilling the goal proposed in each response, thereby reducing desirability and affecting fitting [62]. The optimal conditions for the preparation of

an Al/Co-PILC catalyst active in the SR-AOP degradation of organic contaminants at circumneutral pH yielded by the statistical design of experiments were: AMR_{Co} (%) = 15, $HR_{Eq.}$ (mol OH^-/mol metals) = 2.18 and $T_{Cal.}$ (°C) = 400. However, the previous discussion which detailed the physico-chemical properties obtained from each preparation variable should be considered, as well as the fact that samples prepared with 10% Co in the intercalating solution performed the best, not only in terms of structure (greater expansion, better surface and microporous content), but also in terms of catalytic response in the phenol degradation. The optimal preparation conditions are therefore very close to those of the Co_{10} Al_{90}(2)-400 sample, which are in any case within the optimal range (desirability > 0.8) defined by the contour diagram (figure 6b).

3.4. Catalytic response of the materials in the phenol degradation at circumneutral pH

The catalytic performance of clays modified with Al/Co in the degradation of phenol at circumneutral pH via the activation of sodium PS, was one of the experimental responses used in the statistical design of experiments. Phenol is an excellent molecule to model the reactivity of the least biodegradable organic load in wastewater. A plausible catalytic pathway explaining the degradation comprises the generation of radicals by the activation of PS, according to equation (3.1), where S represents the catalyst's surface. The initial mechanism involves electron transfer between the oxidized cobalt sites on the catalyst surface and the persulfate anions ($S_2O_8^{2-}$), which, after homolytic cleavage of the O–O bonds, leads to the formation of sulfate radicals ($SO_4^{\bullet -}$) under near-neutral pH conditions [31,35,64]. Also, the presence of hydroxide ions (HO^-) promotes generation of hydroxyl radicals ($HO^\bullet$) according to equations (3.2) and (3.3); these hydroxyl radicals, although secondary in their contribution under said pH conditions, can be thought to actively participate in the degradation of the contaminant.

$$\text{S-Co}^{2+} + S_2O_8^{2-} \rightarrow SO_4^{\bullet -} + \text{S-Co}^{3+} + SO_4^{2-} \tag{3.1}$$

$$SO_4^{\bullet -} + HO^- \rightarrow SO_4^{2-} + HO^\bullet \tag{3.2}$$

$$SO_4^{\bullet -} + H_2O \rightarrow SO_4^{2-} + HO^\bullet + H^+ \tag{3.3}$$

A plausible mechanism for phenol removal in the Al/Co-PILC/PS system involves the adsorption of phenol onto the catalyst surface via electrostatic and π–π stacking interactions, followed by their rapid reaction with oxidizing radicals equation (3.4). In accordance with scientific literature on phenol degradation by AOPs [28,65–67], the initial attack on phenol generates hydroxycyclohexadienyl and phenoxyl radicals ($C_6H_6O^\bullet$) through an electron transfer process between phenol and $SO_4^{\bullet -}$ radicals. The subsequent hydroxylation of the aromatic ring and its reaction with O_2 form more stable compounds such as catechol and hydroquinone. Hydrogen abstraction, facilitated by the reduction of Co or by the sulfate radicals, leads to intermediates such as p-benzoquinone or o-benzoquinone. Finally, ring opening produces short-chain aliphatic carboxylic acids (oxalic, acetic, formic, maleic), which can be mineralized in minor extent [65,68]. It is worth noting that these intermediates and reaction by-products have also been extensively reported in the phenol oxidation pathway by the Fenton and photo-Fenton processes based on hydroxyl radicals ($HO^\bullet$) [69,70]. On the other hand, it has been recently evidenced that in PS-based AOPs, both radical species (primarily sulfate, hydroxyl and superoxide radicals) and non-radical species (mainly singlet oxygen, high-valent metal-oxo mediated electron transfer and surface-bound radicals) play a central role in the pollutant's degradation [71]. In our study, in the presence of the best catalyst intermediates such as catechol (0.16 mg l^{-1}), hydroquinone (0.12 mg l^{-1}) and p-benzoquinone (0.18 mg l^{-1}) were recorded at early stages of reaction, as well as aromatic ring cleavage derivatives, such as maleic acid (1.17 mg l^{-1}), acetic acid (1.27 mg l^{-1}) and oxalic acid (1.17 mg l^{-1}), which accumulated at higher concentrations at the final time of reaction (figure 7d), which can be truly considered reaction by-products. Although some of these compounds, especially the aromatic ones, exhibit greater toxicity than phenol itself, owing to their irritant, cytotoxic or potentially mutagenic properties, their just transient presence through the oxidizing degradation underscores the high effectiveness of the catalytic process [72,73]. Besides, low-molecular-weight carboxylic acids such as oxalic and acetic, although may contribute to medium acidification and potentially exert adverse effects on aquatic organisms if accumulate [74], are significantly less toxic than the aromatic intermediates and phenol. These results indicate that the oxidation of phenol by the Al/Co-PILC/PS system, via sulfate radicals, follows a pathway towards low molecular weight compounds, which explains the high measured percentages of phenol degradation and dissolved organic carbon mineralization, even at very short reaction times.

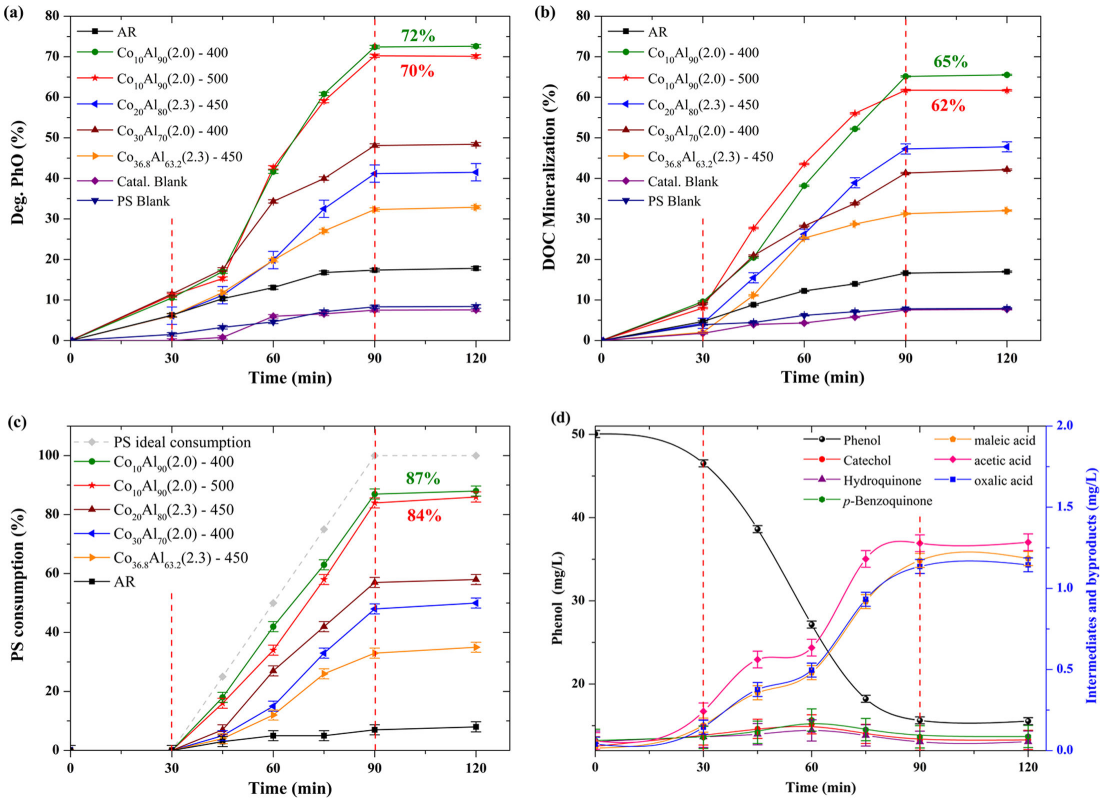

Figure 7. Catalytic behaviour of selected materials during the conversion of phenol via PS activation: (a) phenol (PhO) degradation; (b) DOC mineralization; (c) PS consumption; and (d) concentration of detected phenol oxidation intermediates and by-products in the presence of Al/Co-PILC ($Co_{10}Al_{90}$(2.0)-400). $[PhO]_0$= 50 mg l^{-1} (DOC: 38.3 mg l^{-1}); PS dosage: 35.0 mg PS mg^{-1} DOC (5.63 mmol l^{-1}), V_{PS} added: 0.1 l; catalyst dosage Al/Co-PILC: 0.005 mg Co mg^{-1} PS; *T*: 25.0 ± 0.1 °C; atmospheric pressure = 76 kPa; pH_0: 7.0; PS addition time (between red dotted lines): 60 min.

$$(SO_4^{\bullet -} \text{ or } HO^{\bullet}) + C_6H_5OH \rightarrow C_6H_5O^{\bullet} + (H_2O \text{ or } HSO_4^-) \quad (3.4)$$

The phenol degradation achieved by each solid is listed in table 2. The samples that performed the best in terms of the degradation of phenol and the mineralization of the starting dissolved organic carbon are compared in figure 7a,b, respectively. The Al/Co modified materials offered a significant increase in phenol degradation from the 16.5% exhibited by the starting mineral AR to a maximum degradation of 72.0% and a maximum DOC mineralization of 65% (8.64%, for AR), after only 60 min of reaction under very mild conditions of temperature and pressure. As it can be seen, the samples prepared with a 10% Co molar fraction and the lowest hydrolysis ratio exhibited the best catalytic response in terms of both degradation of phenol and mineralization of DOC, almost regardless of the final calcination temperature of the clay. This suggests, there is a tight correlation between the catalytic response in this reaction and the physico-chemical properties recorded for the same solids, particularly the highest values of d_{001} basal spacing (17.4–18.4 Å) which significantly enhanced the accessibility of the organic substrates to the active sites, and the microporous surface area ($S_{\mu p}$: 134–140 m^2 g^{-1}) which provided greater dispersion of the catalytic active sites. This is presumably owing to the successful condensation of mixed Al/Co polycations in the hydrolysed solution and, later, their intercalation in the form of Al/Co pillars within the aluminosilicate's interlayer. Such a close correlation suggests that the catalytic response of cobalt in Al/Co-PILCs is strongly conditioned by the facility by which organic substrates can access the transition metal, which is predominantly stabilized in the interlayer of the material [8,9]. By contrast, materials prepared with Co fractions greater than or equal to 20% exhibited highly variable catalytic performance both in terms of phenol degradation (21–63%) and DOC mineralization (31–64%). This reveals that, although cobalt exhibits its greatest reactivity in the materials studied when it is intercalated mostly in the form of mixed Al/Co pillars, cobalt oxides on the surface that interact at different extent with the aluminosilicate support also display a response. This behaviour was also observed in the CoO_x/Al-PILC reference microencapsulated material, where the incorporation of cobalt and the moderate increase in the physico-chemical properties of the solid enhanced the

catalytic performance in terms of phenol degradation (62%) and DOC mineralization (53%); however, higher concentrations of cobalt (0.103 mg l^{-1}) leached into the treated water, which also occurred in the case of the materials modified with Co atomic fractions greater than 20% (approx. 0.02–0.05 mg l^{-1}). This suggests the efficiency of these materials particularly at degrading and mineralizing the substrates was rather more owing to activation of the oxidizing agent by the dissolved fraction of the transition metal (homogeneous phase). No concentration of cobalt at all is desirable in surface waters, a requirement even more stringent in drinking water. It is then auspicious that the materials here investigated both performed better at degrading phenol, but at the same time demonstrated greater cobalt stability against leaching under the reaction conditions (approx. 0.012 mg Co l^{-1}); this also represents an advantage over other cobalt-based materials reported, which exhibited higher leaching even at circumneutral pH (approx. 0.06–0.85 mg l^{-1}) [66,75,76]. It strongly merits further studies to optimize the catalytic response of the Al/Co-clay catalyst, to establish the optimal reaction conditions for degradation of different organic contaminants. These materials could therefore be suitable for the treatment of contaminant wastewater before its final discharge.

The statistical effect of the experimental variables on phenol degradation is illustrated by the response surface and contour plot in figure 8. As with the simultaneous evaluation of all the responses studied, the catalytic response shows the same trend, favouring the lowest values of AMR_{Co} (close to 10%) and $HR_{Eq.}$ (close to 2.0) evaluated. The control experiment using PS only (PS blank, without the addition of the catalyst) demonstrated the essential role of the catalyst in activating the oxidizing agent, given that neither the degradation of phenol nor the DOC mineralization exceeded 10.0% in such conditions. This indicates that the removal of the contaminant occurred mainly through the catalytic activation of PS towards sulfate radicals, and not by the direct attack of PS on the organic substrate. Similarly, when the blank experiment (Catal. Blank, without addition of PS) was carried out in the presence of the Co_{10} Al_{90}(2)-400 catalyst, values of phenol degradation and DOC mineralization were only around 10.0%, demonstrating that the adsorption of phenol alone on the catalyst surface is not enough to explain the decrease in the concentration of the contaminant. Therefore, the joint attack of organic substrates by PS follows a predominantly catalytic mechanism for the formation of radical species responsible for the degradation of phenol and the DOC mineralization.

The transition metal demonstrated a high catalytic response, mainly where it was stabilized in the form of Al/Co pillars. It activated the persulfate towards powerful oxidizing $SO_4^{\bullet-}$ sulfate radicals under circumneutral pH conditions that are typical of both domestic and industrial waste waters. The percentages of PS consumed (figure 7c) for the same catalytic tests demonstrated that, indeed, the materials intercalated with 10% Co solutions and a $HR_{Eq.}$ of 2.0, in addition to exhibiting the greatest degradation of phenol and DOC, also displayed a PS consumption close to 90%. Furthermore, the PS consumption pattern was almost identical to the ideal consumption, considering the rate of PS addition used in this series of experiments. This suggests that in the presence of correctly expanded Al/Co-PILCs, the activation rate of the oxidizing agent is very high and therefore the maximum degradation of the contaminant could be achieved in even shorter reaction times if the initial concentration of the oxidizing agent is increased. The degradation rate could also be improved by faster or complete addition of the oxidizing agent at earlier time of reaction; as previously reported, the degradation rate of the contaminants appears to significantly increase when PS is introduced at the beginning of the catalytic reaction, suggesting higher reaction kinetics (pseudo-first-order rate constant, k: 0.38–0.046 min^{-1}) [75–77] and greater generation of reactive species ($SO_4^{\bullet-}$ and $HO^{\bullet}$) in the system. By contrast, in Fenton-type systems, the addition of hydrogen peroxide at a constant flow, as slow as possible, has shown to favour better utilization of the oxidant in the degradation of the contaminants [13,62,78].

The zero-charge point (pH_{pzc}) of the $Co_{10}Al_{90}$(2)-400 catalyst was 5.37 (electronic supplementary material, figure S7), a value slightly higher than that exhibited by Al/Fe-PILCs for the same starting clay [79]. Therefore, since the catalytic tests were carried out at a pH close to 7.0, the catalyst surface was negatively charged. Considering the high pKa of the phenol molecule (approx. 10) [80], in the pH conditions in which the catalytic tests were carried out, more than 99.9% of the dissolved phenol was in its molecular form, meaning that the observed responses were not owing to electrostatic interactions between the model molecule and the catalyst surface.

To evaluate the reusability of the Al/Co-PILC catalyst, the material with the best physico-chemical properties and catalytic performance ($Co_{10}Al_{90}$(2.0)-400) was used through five consecutive cycles for the degradation of phenol (figure 9). After such a set of cycles, a 12% reduction in the phenol degradation, alongside a decrease close to 36% in DOC mineralization, were recorded. Since, as said, the metal leaching was negligible, this decrease could be then mostly attributed to chemisorption of reaction intermediates or by-products on the catalyst surface, particularly low molecular weight

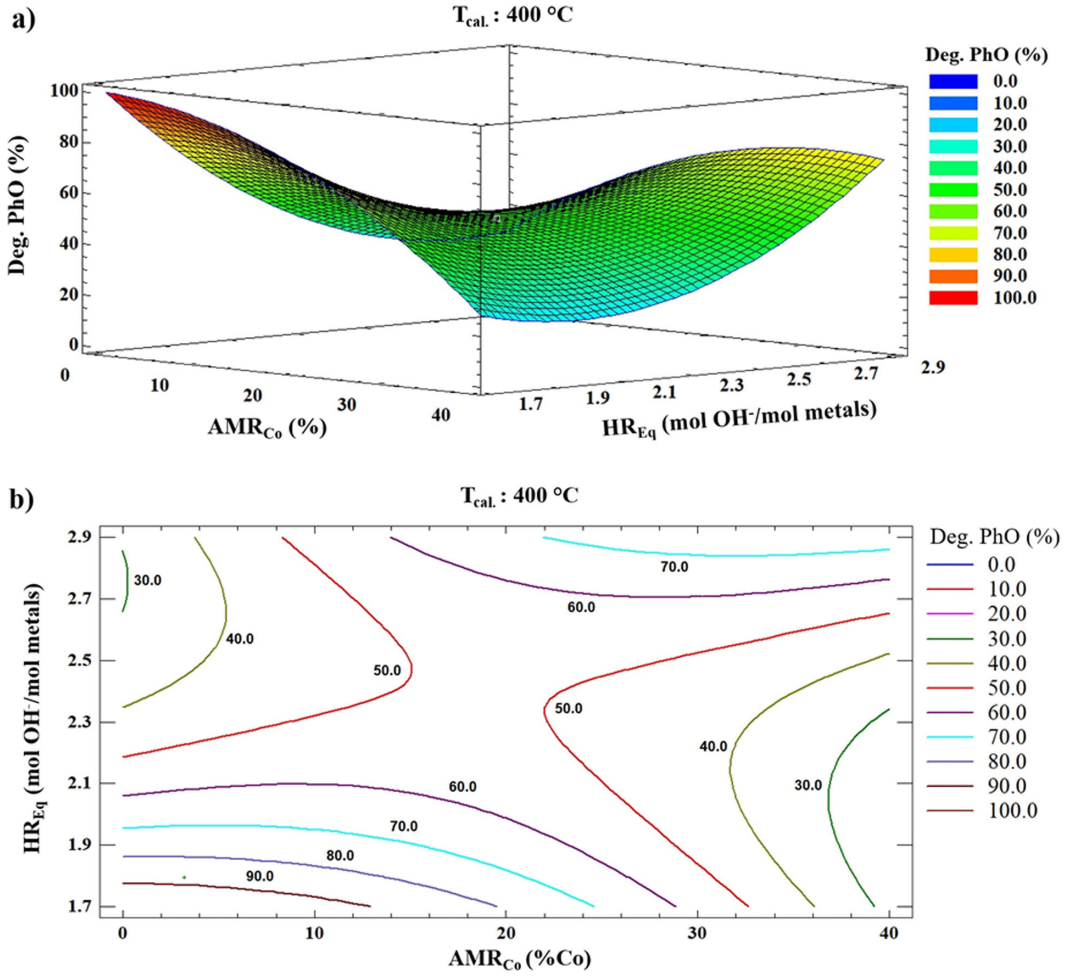

Figure 8. Catalytic response of the prepared materials in the degradation of phenol (PhO): (a) response surface and (b) contour diagram.

carboxylic acids previously reported like strongly refractory against the chemical oxidation [81–84]. These compounds can block active sites within the catalyst pores, limiting the deep conversion of starting and transient substrates into CO_2. It correlates with both the significant decrease (approx. 50%) in the textural properties of the catalyst, and a reduction of the PS consumption (approx. 48%) (electronic supplementary material, table S5). The low leaching of cobalt and aluminium after five catalytic cycles (0.001 mg l^{-1}) demonstrated the high chemical stability of the active sites under reaction conditions. The extremely low leaching of metal ions thus confirms that the structural mixed pillars remained stable during operation and that the catalyst does not introduce significant secondary metal contamination into the treated water. Furthermore, since the dissolved cobalt concentrations are much lower than those required to support homogeneous activation of the PS, the results allow to conclude that the observed degradation of phenol primarily proceeds via a heterogeneous catalytic pathway, in which the surface Co sites act as active centres for generation of the oxidizing species. Thus, the observed loss of activity over the cycles is better explained by the accumulation of refractory carboxylic acids on the catalyst's surface and not by the dissolution of the active metal. However, further studies under different reaction conditions are needed to corroborate the predominantly heterogeneous nature of the process and clarify the role of persistent by-products in modulating the catalytic response.

Finally, it is important to highlight that in this study very low doses of active metal in the catalyst (6.7 mg Co l^{-1}) and PS (5.63 mmol l^{-1}) were used to obtain the greatest possible difference between the catalytic response of the prepared materials. Moreover, in comparison with several recently reported cobalt-based catalysts, for example, a CuO_x@Co-LDH-type catalyst demonstrated 100% phenol degradation in 40 min of reaction in the presence of 300 mg catalyst l^{-1} and 5 mmol PS l^{-1} [85]; however, the organic carbon mineralization efficiency was not reported, and although Co leaching was mentioned as very low, Cu leaching should also be considered in this case. On the other hand, a 96% degradation of bisphenol A (BPA) and around 40% TOC removal in 60 min of reaction was

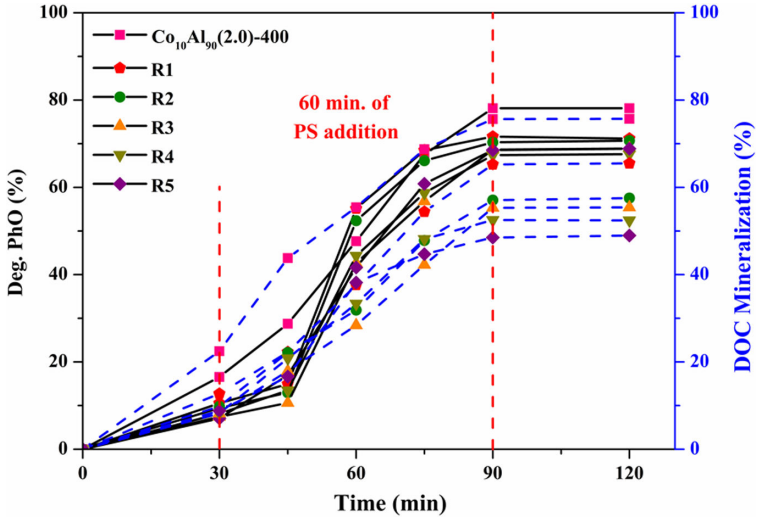

Figure 9. Reusability tests of the $Co_{10}Al_{90}$(2.0)-400 catalyst after five cycles of phenol degradation: $[PhO]_0 = 50$ mg l^{-1} (DOC: 38.3 mg l^{-1}); PS dosage: 35.0 mg PS/mg DOC (5.63 mmol l^{-1}), V_{PS} added: 0.1 l; dosage of the Al/Co-PILC catalyst: 0.025 mg Co/mg PS; *T*: 25.0 ± 0.1 °C; atmospheric pressure = 76 kPa; pH_0: 7.0; PS addition time (between the red dotted lines): 60 min. Phenol degradation (bulk lines); DOC mineralization (dotted lines).

also recently reported, in the presence of 200 mg l^{-1} of a $CoFe_2O_4$ type catalyst and PMS [86], but not negligible leaching of 0.146 mg Co l^{-1} and 0.026 mg Fe l^{-1} was found. Therefore, the Al/Co-PILC catalyst exhibits a very high reactivity per mole of cobalt, which clearly rivals the best catalysts reported so far in the degradation of various pollutants by sulfate radicals. Furthermore, the optimal conditions to achieve maximum phenol degradation and DOC mineralization in the shortest possible reaction time should be determined in a subsequent study based on the catalyst loading and PS dosage, as has been done in previous studies for other modified clays [13,62]. This new approach based on the SR-AOP/Al/Co-PILCs system displays significant advantages as compared with traditional degradation methods, thanks to the higher selectivity exhibited by the sulfate radicals, its ability breaking wider range of organic functionalities and contaminants, and its broader operational range of pH, which is also ideal under circumneutral conditions. As the large-scale preparation of the Al/Fe-PILC catalyst has proven to be highly effective for the Fenton treatment of organic contaminants in wastewater, the preparation of the Al/Co-PILC catalyst is also an attractive opportunity for future applications in the treatment of industrial wastewater.

On the other hand, a key disadvantage that still needs to be addressed, not only in Al/Co-PILCs but in all cobalt-based active catalysts in SR-AOPs, is metal leaching, which, although low in the Al/Co-PILC (approx. 0.011 mg l^{-1}), can play a crucial environmental role owing to the high toxicity of this metal. This is because of its easy bioaccumulation in aquatic organisms and its potential to affect cellular processes by *in situ* generating reactive oxygen species, enzymatic alterations and genotoxic effects [87–89]. Nevertheless, this risk can be considered compensated in the treatment of waters contaminated with highly toxic compounds, and/or with very high loads of dissolved organic pollution, such as landfill leachates, industrial wastewater and hospital wastewater, among other highly polluting effluents of natural water bodies. By contrast, of course, its use in water purification for human consumption is not recommended under any circumstances, given the need to ensure strict absence of this type of metals in the final product. The application of the SR-AOP technology represents a promising approach for the treatment of industrial effluents containing recalcitrant organic pollutants. Its ability to generate highly reactive sulfate radicals allows for the effective removal of compounds such as dyes, phenols, aromatic hydrocarbons and pesticides, found in wastewater from sectors like textiles, petrochemicals and pharmaceuticals [90–93]. Unlike other oxidation methods, this technology does not require drastic pH adjustments and maintains high performance even under circumneutral conditions, making it adaptable to various types of effluents without the need for complex pre-treatments. Therefore, given the great potential of pillared clays and their outstanding physico-chemical properties, a more detailed study could optimize their long-term application, establishing them as an efficient and sustainable system for degradation of contaminants in water.

Despite the excellent physico-chemical and catalytic properties of the Al/Co-PILCs described thus far, the incorporation of higher amounts of highly reactive cobalt (by means of truly mixed Al/Co

pillars) into this type of solid remains an opportunity for improvement to facilitate their exploitation in large-scale catalytic solutions. It is also advisable to conduct a more in-depth physico-chemical characterization of the active sites responsible for the high reactivity of cobalt in these structures using techniques such as cyclic voltammetry (CV) and electrochemical impedance spectroscopy (EIS); these techniques could provide key information on the electron transfer mechanisms involved in this catalytic system [17]. Besides, although cobalt oxides are not intrinsically ferromagnetic, since in our materials Co is expected to be mostly stabilized doping alumina nanoparticles (the Al/Co pillars), under very specific conditions (namely nanostructured oxides, substitution of Al^{3+} sites within the alumina framework), they may exhibit weak ferromagnetism; this undoubtedly would merit such additional determinations to further characterize Al/Co-PILCs. Future studies should also include the identification of a greater number of intermediates during phenol degradation, using liquid chromatography-mass spectrometry (LC-MS) and gas chromatography-mass spectrometry (GC-MS), tools that would more clearly elucidate the mechanism and change in toxicity of wastewater streams as treated by the Al/Co-PILC/PS catalytic system. Finally, a study of the catalytic system in the presence of radical scavenging species is desirable to unequivocally establish the oxidizing radical species involved in the degradation of organic pollutants by this catalytic system under near-neutral pH conditions, and to incorporate toxicity assays during the monitoring of the oxidative process, in order to broadly evaluate its potential for the remediation of environmental pollution, primarily that caused by wastewater (industrial, domestic, hospital).

4. Conclusion

This work reports for the first time the successful preparation of pillared clays containing Al/Co (Al/Co-PILCs) from highly concentrated hydrolysed mixed solutions of both metals. A combination of statistical process optimization tools and physico-chemical characterization techniques (mainly powder-XRD, N_2-sorptometry, H_2-TPR, TGA/DSC and DR-UV-vis) were used for the study. The atomic molar ratio of Co (AMR_{Co}) in the mixed Al–Co intercalating solutions exhibited the most statistically significant effect on the formation of stable polycations with a high interlayering power. The material prepared with 10% Co, together with the lowest values of $HR_{Eq.}$ (2.0) and $T_{Cal.}$ (400°C) displayed the best physico-chemical characteristics (d_{001}: 18.4 A, S_{BET}: 194 $m^2\ g^{-1}$, $S_{\mu p}$: 140 $m^2\ g^{-1}$). Despite the low metal uptake, the final Co content (0.404% w/w) was much higher than that documented to date when this type of materials has been correctly expanded from diluted precursors. By contrast, there was no effective expansion of the clay in the materials prepared with an AMR_{Co} greater than or equal to atomic 20%, although they did show an increase in the specific surface area associated with the formation of Co oxides on the surface, which besides exhibited lower chemical stability in the targeted catalytic reaction. The most promising Al/Co-PILC ($Co_{10}Al_{90}$(2)-400) demonstrated an excellent degradation of phenol (72%) and mineralization of dissolved organic carbon (65%) in just 60 min of reaction time at ambient pressure (76 kPa) and temperature (25°C), and negligible leaching of cobalt in the treated water (0.011 mg l^{-1}). The progressive addition of PS at circumneutral pH led to the rapid activation of this oxidizing agent towards sulfate radicals, requiring a very low dose of the active metal in the catalyst (0.005 mg Co/mg PS; approx. 1.73 g catalyst l^{-1}). The quick consumption of the added PS suggests the speed of the contaminant's degradation can be further optimized by reducing the time in which the oxidizing agent is added to the catalytic system, thereby helping the studied materials better eliminate dissolved organic contaminants in industrial and other highly toxic water contaminants. Although the results demonstrate remarkable efficiency of Al/Co-PILCs prepared from highly concentrated precursors in the removal of phenol by sulfate radicals, and a clear trend towards deep mineralization of dissolved organic carbon, the catalytic system has the following main limitations: *(i)* rapid deactivation during reuse attributed to the blocking of active sites by light carboxylic acids as oxidation by-products that accumulate; and *(ii)* the limited cobalt content that can be stabilized by true mixed Al/Co pillars. Future work on this catalytic system should then focus on: *(i)* determining simple conditions for catalyst reactivation upon reuse; *(ii)* studying in more detail the oxidative pathway of phenol and other recalcitrant molecules in wastewater, such as some hazardous medicines and pesticides, using chromatographic techniques coupled with mass spectrometry, namely LC-MS, GC-MS and ion chromatography; and *(iii)* establishing the optimal reaction conditions for the Al/Co-PILC/PS catalytic system that maximize degradation and mineralization of emerging-concern contaminants commonly present in wastewater in the shortest possible time of reaction.

Ethics. This work did not require ethical approval from a human subject or animal welfare committee.

Data accessibility. Supporting data and figures have been included in the article's electronic supplementary material.

Supplementary material is available online [94].

Declaration of AI use. We have not used AI-assisted technologies in creating this article.

Authors' contributions. J.S.T.-R.: formal analysis, investigation, writing—original draft; O.J.C.-M.: investigation, writing—original draft; A.M.G.-M.: formal analysis, methodology, validation, writing—review and editing; A.H.-T.: conceptualization, data curation, validation, writing—review and editing; L.-A.G.: conceptualization, formal analysis, funding acquisition, project administration, supervision, writing—review and editing.

All authors gave final approval for publication and agreed to be held accountable for the work performed therein.

Conflict of interest declaration. We declare we have no competing interests.

Funding. This work was supported by Vicerrectoría de Investigación e Interacción Social VIIS—Universidad de Nariño (project code 2284).

References

1. Zhu TT, Zhou CH, Kabwe FB, Wu QQ, Li CS, Zhang JR. 2019 Exfoliation of montmorillonite and related properties of clay/polymer nanocomposites. *Appl. Clay Sci*. **169**, 48–66. (doi:10.1016/j.clay.2018.12.006)
2. Zhou C, Tong D, Yu W. 2019 Smectite nanomaterials: preparation, properties, and functional applications. In *Nanomaterials from clay minerals* (eds A Wang, W Wang), pp. 335–364. Amsterdam, The Netherlands: Elsevier. (doi:10.1016/B978-0-12-814533-3.00007-7)
3. Vicente MA, Gil A, Bergaya F. 2013 Chapter 7.5 Pillared clays and clay minerals. In *Developments in clay science* (eds F Bergaya, G Lagaly), pp. 393–421. Amsterdam, The Netherlands: Elsevier.
4. Galeano LA, Vicente MÁ, Gil A. 2014 Catalytic degradation of organic pollutants in aqueous streams by mixed Al/M-pillared clays (M = Fe, Cu, Mn). *Catal. Rev*. **56**, 239–287. (doi:10.1080/01614940.2014.904182)
5. Khankhasaeva STs, Dashinamzhilova ETs, Dambueva DV. 2017 Oxidative degradation of sulfanilamide catalyzed by Fe/Cu/Al-pillared clays. *Appl. Clay Sci*. **146**, 92–99. (doi:10.1016/j.clay.2017.05.018)
6. Ning S, Huang S, Yang H, Zhao B, Su Y. 2023 Bimetal catalyst based on Fe and Co supported on Al pillared interlayer clays: preparation, reactivity and mechanism for SCR-CH_4. *iScience* **26**, 107432. (doi:10.1016/j.isci.2023.107432)
7. Bergaya F, Lagaly G. 2013 Chapter 1 General introduction: clays, clay minerals, and clay science. In *Developments in clay science* (eds F Bergaya, G Lagaly), pp. 1–19. Amsterdam, The Netherlands: Elsevier. (doi:10.1016/B978-0-08-098258-8.00001-8)
8. Muñoz HJ, Vallejo C, Blanco C, Gil A, Vicente MÁ, Ramírez JH, Galeano LA. 2018 10 kg scaled-up preparation of Al/Fe-pillared clay CWPO catalysts from concentrated precursors. *Green Chem*. **20**, 5196–5208. (doi:10.1039/c8gc02445f)
9. Vallejo CA, Galeano LA, Trujillano R, Vicente MÁ, Gil A. 2020 Preparation of Al/Fe-PILC clay catalysts from concentrated precursors: enhanced hydrolysis of pillaring metals and intercalation. *RSC Adv*. **10**, 40450–40460. (doi:10.1039/d0ra08948f)
10. Galeano LA, Gil A, Vicente MA. 2010 Effect of the atomic active metal ratio in Al/Fe-, Al/Cu- and Al/(Fe–Cu)-intercalating solutions on the physicochemical properties and catalytic activity of pillared clays in the CWPO of methyl orange. *Appl. Catal. B* **100**, 271–281. (doi:10.1016/j.apcatb.2010.08.003)
11. Gómez-Obando VA, García-Mora AM, Basante JS, Hidalgo A, Galeano LA. 2019 CWPO degradation of methyl orange at circumneutral pH: multi-response statistical optimization, main intermediates and by-products. *Front. Chem*. **7**, 772. (doi:10.3389/fchem.2019.00772)
12. Ramírez JH, Galeano LA, Pinchao G, Bedoya RA, Hidalgo A. 2018 Optimized CWPO phenol oxidation in CSTR reactor catalyzed by Al/Fe-PILC from concentrated precursors at circumneutral pH. *J. Environ. Chem. Eng*. **6**, 2429–2441. (doi:10.1016/j.jece.2018.02.024)
13. García-Mora AM, Portilla-Delgado CS, Torres-Palma RA, Hidalgo-Troya A, Galeano LA. 2021 Catalytic wet peroxide oxidation to remove natural organic matter from real surface waters at urban and rural drinking water treatment plants. *J. Water Process Eng*. **42**, 102136. (doi:10.1016/j.jwpe.2021.102136)
14. Ramírez JH, Galeano LA. 2019 Natural organic matter removal by heterogeneous catalytic wet peroxide oxidation (CWPO). In *Applications of advanced oxidation processes (AOPs) in drinking water treatment* (eds A Gil, LA Galeano, MA Vicente), pp. 69–98. Cham, Switzerland: Springer International Publishing. (doi:10.1007/698_2017_122)
15. Marković M, Marinović S, Mudrinić T, Mojović Z, Ajduković M, Milutinović-Nikolić A, Banković P. 2018 Cobalt impregnated pillared montmorillonite in the peroxymonosulfate induced catalytic oxidation of tartrazine. *React. Kinet. Mech. Catal*. **125**, 827–841. (doi:10.1007/s11144-018-1466-1)
16. Milovanović B, Marinović S, Vuković Z, Milutinović-Nikolić A, Petrović R, Banković P, Mudrinić T. 2022 The influence of cobalt loading on electrocatalytic performance toward glucose oxidation of pillared montmorillonite-supported cobalt. *J. Electroanal. Chem*. **915**, 116332. (doi:10.1016/j.jelechem.2022.116332)
17. Mudrinić T, Marinović S, Milutinović-Nikolić A, Jović-Jovičić N, Ajduković M, Mojović Z, Banković P. 2019 Novel non-enzymatic glucose sensing material based on pillared clay modified with cobalt. *Sensors Actuators B* **299**, 126976. (doi:10.1016/j.snb.2019.126976)
18. Amaya MG, García Blanco AA, Toncón-Leal C, Sapag K. 2021 Incorporation of Co in different stages of the synthesis of Al-PILC and its effect as a Fischer–Tropsch catalyst. *Ind. Eng. Chem. Res*. **60**, 18929–18937. (doi:10.1021/acs.iecr.1c03791)

19. Darmawan A, Widiarsih A. 2018 Aluminium - cobalt-pillared clay for dye filtration membrane. *IOP Conf. Ser.: Mater. Sci. Eng* **349**, 012002. (doi:10.1088/1757-899X/349/1/012002)
20. Su H, Zeng S, Dong H, Du Y, Zhang Y, Hu R. 2009 Pillared montmorillonite supported cobalt catalysts for the Fischer–Tropsch reaction. *Appl. Clay Sci*. **46**, 325–329. (doi:10.1016/j.clay.2009.09.002)
21. Zhao YH *et al*. 2015 Cobalt-supported carbon and alumina co-pillared montmorillonite for Fischer–Tropsch synthesis. *Fuel Process. Technol*. **138**, 116–124. (doi:10.1016/j.fuproc.2015.05.019)
22. Kollár M, De Stefanis A, Solt HE, Mihályi MR, Valyon J, Tomlinson AAG. 2010 The mechanism of the Fischer–Tropsch reaction over supported cobalt catalysts. *J. Mol. Catal*. **333**, 37–45. (doi:10.1016/j.molcata.2010.09.014)
23. Marković M, Marinović S, Mudrinić T, Ajduković M, Jović-Jovičić N, Mojović Z, Orlić J, Milutinović-Nikolić A, Banković P. 2019 Co(II) impregnated Al(III)-pillared montmorillonite–synthesis, characterization and catalytic properties in Oxone® activation for dye degradation. *Appl. Clay Sci*. **182**, 105276. (doi:10.1016/j.clay.2019.105276)
24. Vicente MA, Belver C, Trujillano R, Rives V, Álvarez AC, Lambert JF, Korili SA, Gandía LM, Gil A. 2004 Preparation and characterisation of Mn- and Co-supported catalysts derived from Al-pillared clays and Mn- and Co-complexes. Appl. Catal. A Gen. **267**, 47–58. (doi:10.1016/j.apcata.2004.02.023)
25. Moronta A, Troconis ME, González E, Morán C, Sánchez J, González A, Quiñónez J. 2006 Dehydrogenation of ethylbenzene to styrene catalyzed by Co, Mo and CoMo catalysts supported on natural and aluminum-pillared clays. *Appl. Catal. A Gen.* **310**, 199–204. (doi:10.1016/j.apcata.2006.06.003)
26. Thomas SM, Bertrand JA, Occelli ML, Stencel JM, Gould SAC. 1999 Synthesis and characterization of expanded smectites containing trinuclear Co complexes. *Chem. Mater*. **11**, 1153–1164. (doi:10.1021/cm9811141)
27. Urruchurto CM, Carriazo JG, Osorio C, Moreno S, Molina RA. 2013 Spray-drying for the preparation of Al–Co–Cu pillared clays: a comparison with the conventional hot-drying method. *Powder Technol*. **239**, 451–457. (doi:10.1016/j.powtec.2013.02.033)
28. Banković P, Mojović Z, Milutinović-Nikolić A, Jović-Jovičić N, Marinović S, Jovanović D. 2010 Mixed pillared bentonite for electrooxidation of phenol. *Appl. Clay Sci*. **49**, 84–89. (doi:10.1016/j.clay.2010.04.012)
29. Mojović Z, Banković P, Milutinović-Nikolić A, Nedić B, Jovanović D. 2010 Co-aluminosilicate based electrodes. *Appl. Clay Sci*. **48**, 179–184. (doi:10.1016/j.clay.2009.11.022)
30. Bertella F, Pergher SBC. 2015 Pillaring of bentonite clay with Al and Co. *Microporous Mesoporous Mater*. **201**, 116–123. (doi:10.1016/j.micromeso.2014.09.013)
31. Giannakis S, Lin KYA, Ghanbari F. 2021 A review of the recent advances on the treatment of industrial wastewaters by sulfate radical-based advanced oxidation processes (SR-AOPs). *Chem. Eng. J*. **406**, 127083. (doi:10.1016/j.cej.2020.127083)
32. Liu Y, Chen X, Yang Y, Feng Y, Wu D, Mao S. 2019 Activation of persulfate with metal–organic framework-derived nitrogen-doped porous Co@C nanoboxes for highly efficient p-chloroaniline removal. *Chem. Eng. J*. **358**, 408–418. (doi:10.1016/j.cej.2018.10.012)
33. Nguyen TB, Doong Ra, Huang CP, Chen CW, Dong CD. 2019 Activation of persulfate by CoO nanoparticles loaded on 3D mesoporous carbon nitride (CoO@meso-CN) for the degradation of methylene blue (MB). *Sci. Total Environ*. **675**, 531–541. (doi:10.1016/j.scitotenv.2019.04.230)
34. Li B, Wang YF, Zhang L, Xu HY. 2022 Enhancement strategies for efficient activation of persulfate by heterogeneous cobalt-containing catalysts: a review. *Chemosphere* **291**, 132954. (doi:10.1016/j.chemosphere.2021.132954)
35. Oh WD, Dong Z, Lim TT. 2016 Generation of sulfate radical through heterogeneous catalysis for organic contaminants removal: current development, challenges and prospects. *Appl. Catal. B* **194**, 169–201. (doi:10.1016/j.apcatb.2016.04.003)
36. Hama Aziz KH, Mustafa FS, Karim MAH, Hama S. 2025 Pharmaceutical pollution in the aquatic environment: advanced oxidation processes as efficient treatment approaches: a review. *Mater. Adv.* **6**, 3433–3454. (doi:10.1039/D4MA01122H)
37. Jiang HZ, Huang ZH, Wang L, Guo ZY, Zhang P, Wang J, Ji ZY. 2026 The choice of treatment of antibiotic wastewater by sulfate radical-based advanced oxidation processes: peroxymonosulfate (PMS) or peroxydisulfate (PDS). *Chem. Eng. Sci*. **320**, 122629. (doi:10.1016/j.ces.2025.122629)
38. Cardona Y, Węgrzyn A, Miśkowiec P, Korili SA, Gil A. 2022 Catalytic photodegradation of organic compounds using TiO_2/pillared clays synthesized using a nonconventional aluminum source. *Chem. Eng. J*. **446**, 136908. (doi:10.1016/j.cej.2022.136908)
39. Gong Z, Liao L, Lv G, Wang X. 2016 A simple method for physical purification of bentonite. *Appl. Clay Sci*. **119**, 294–300. (doi:10.1016/j.clay.2015.10.031)
40. Muñoz HJ, Blanco C, Gil A, Vicente MÁ, Galeano LA. 2017 Preparation of Al/Fe-pillared clays: effect of the starting mineral. *Materials* **10**, 1364. (doi:10.3390/ma10121364)
41. Galeano LA, Muñoz HJ, García AM, Gil A, Vicente MÁ. 2018 Development of Mn or Fe sulfides in the interlayer space of raw and Al-pillared bentonite. *Appl. Clay Sci*. **157**, 31–40. (doi:10.1016/j.clay.2018.02.022)
42. Čerović LS, Milonjić SK, Bahloul-Hourlier D, Doucey B. 2002 Surface properties of silicon nitride powders. *Colloids Surfaces* **197**, 147–156. (doi:10.1016/s0927-7757(01)00863-9)
43. Liang C, Huang CF, Mohanty N, Kurakalva RM. 2008 A rapid spectrophotometric determination of persulfate anion in ISCO. *Chemosphere* **73**, 1540–1543. (doi:10.1016/j.chemosphere.2008.08.043)
44. Song W, Li J, Wang Z, Fu C, Zhang X, Feng J, Xu Z, Song Q. 2020 Degradation of bisphenol A by persulfate coupled with dithionite: optimization using response surface methodology and pathway. *Sci. Total Environ*. **699**, 134258. (doi:10.1016/j.scitotenv.2019.134258)
45. Rahmati S, Ahmadi A, Hosseini MR, Nasab MM. 2019 Optimization of continuous air-assisted solvent extraction for treating dilute Cu leach solutions using response surface methodology. *Miner. Eng*. **131**, 154–163. (doi:10.1016/j.mineng.2018.11.018)

46. Falahati MT, Ghoreishi SM. 2019 Preparation of Balangu (*Lallemantia royleana*) seed mucilage aerogels loaded with paracetamol: evaluation of drug loading via response surface methodology. *J. Supercrit. Fluids* **150**, 1–10. (doi:10.1016/j.supflu.2019.04.003)
47. Bi S, Wang C, Cao Q, Zhang C. 2004 Studies on the mechanism of hydrolysis and polymerization of aluminum salts in aqueous solution: correlations between the 'Core-links' model and 'Cage-like' Keggin-Al_{13} model. *Coord. Chem. Rev*. **248**, 441–455. (doi:10.1016/j.ccr.2003.11.001)
48. Banković P, Milutinović-Nikolić A, Mojović Z, Jović-Jovičić N, Perović M, Spasojević V, Jovanović D. 2013 Synthesis and characterization of bentonites rich in beidellite with incorporated Al or Al–Fe oxide pillars. *Microporous Mesoporous Mater*. **165**, 247–256. (doi:10.1016/j.micromeso.2012.08.029)
49. Thommes M, Kaneko K, Neimark AV, Olivier JP, Rodriguez-Reinoso F, Rouquerol J, Sing KSW. 2015 Physisorption of gases, with special reference to the evaluation of surface area and pore size distribution (IUPAC Technical Report). *Pure Appl. Chem*. **87**, 1051–1069. (doi:10.1515/pac-2014-1117)
50. Sing KSW. 1985 Reporting physisorption data for gas/solid systems with special reference to the determination of surface area and porosity (recommendations 1984). *Pure Appl. Chem.* **57**, 603–619. (doi:10.1351/pac198557040603)
51. Timofeeva MN, Khankhasaeva STs, Talsi EP, Panchenko VN, Golovin AV, Dashinamzhilova ETs, Tsybulya SV. 2009 The effect of Fe/Cu ratio in the synthesis of mixed Fe,Cu,Al-clays used as catalysts in phenol peroxide oxidation. *Appl. Catal. B* **90**, 618–627. (doi:10.1016/j.apcatb.2009.04.024)
52. Padmakar D, Suresh Babu G, Rajitha P, Lingaiah N. 2022 Understanding the role of SrO-ZrO_2 mixed oxide support for Co_3O_4 based catalysts towards H_2 production from steam reforming of glycerol. *Appl. Surf. Sci*. **606**, 154954. (doi:10.1016/j.apsusc.2022.154954)
53. Reynoso AJ, Iriarte-Velasco U, Gutiérrez-Ortiz MA, Ayastuy JL. 2022 Ce-doped cobalt aluminate catalysts for the glycerol hydrodeoxygenation (HDO) with *in-situ* produced hydrogen. *J. Environ. Chem. Eng*. **10**, 107612. (doi:10.1016/j.jece.2022.107612)
54. Surendar M, Sagar TV, Babu BH, Lingaiah N, Rao KSR, Prasad PSS. 2015 Glycerol steam reforming over La–Ce–Co mixed oxide-derived cobalt catalysts. *RSC Adv*. **5**, 45184–45193. (doi:10.1039/c5ra02837j)
55. Arnoldy P, Moulijn JA. 1985 Temperature-programmed reduction of CoO/Al_2O_3 catalysts. *J. Catal.* **93**, 38–54. (doi:10.1016/0021-9517(85)90149-6)
56. Marinović S, Mudrinić T, Dojčinović B, Barudžija T, Banković P, Novaković T. 2021 Cobalt-doped alumina catalysts in catalytic oxidation of tartrazine induced by Oxone®. *J. Environ. Chem. Eng*. **9**, 106348. (doi:10.1016/j.jece.2021.106348)
57. Li D, Ding Y, Wei X, Xiao Y, Jiang L. 2015 Cobalt-aluminum mixed oxides prepared from layered double hydroxides for the total oxidation of benzene. *Appl. Catal*. **507**, 130–138. (doi:10.1016/j.apcata.2015.09.038)
58. Moogi S, Dasari P, Gundeboyina R, Nakka L, Prasad Potharaju SS, Park YK. 2024 Hydrogen generation from glycerol steam gasification over cobalt loaded MgO–Al_2O_3 hydrotalcite supports. *Int. J. Hydrog. Energy* **52**, 412–423. (doi:10.1016/j.ijhydene.2023.03.184)
59. Pardo-Tarifa F, Cabrera S, Sanchez-Dominguez M, Boutonnet M. 2017 Ce-promoted Co/Al_2O_3 catalysts for Fischer–Tropsch synthesis. *Int. J. Hydrog. Energy* **42**, 9754–9765. (doi:10.1016/j.ijhydene.2017.01.056)
60. Madejová J, Komadel P. 2001 Baseline studies of the clay minerals society source clays: infrared methods. *Clays Clay Miner*. **49**, 410–432. (doi:10.1346/ccmn.2001.0490508)
61. Gil A, Korili SA, Trujillano R, Vicente MA. 2011 A review on characterization of pillared clays by specific techniques. *Appl. Clay Sci*. **53**, 97–105. (doi:10.1016/j.clay.2010.09.018)
62. Garcia-Mora AM, Torres-Palma RA, García H, Hidalgo-Troya A, Galeano LA. 2021 Removal of dissolved natural organic matter by the Al/Fe pillared clay-activated-catalytic wet peroxide oxidation: statistical multi-response optimization. *J. Water Process Eng*. **39**, 101755. (doi:10.1016/j.jwpe.2020.101755)
63. Djomgoue P, Njopwouo D. 2013 FT-IR spectroscopy applied for surface clays characterization. *J. Surf. Eng. Mater. Adv. Technol*. **03**, 275–282. (doi:10.4236/jsemat.2013.34037)
64. Wacławek S, Lutze HV, Grübel K, Padil VVT, Černík M, Dionysiou DD. 2017 Chemistry of persulfates in water and wastewater treatment: a review. *Chem. Eng. J*. **330**, 44–62. (doi:10.1016/j.cej.2017.07.132)
65. Olmez-Hanci T, Arslan-Alaton I. 2013 Comparison of sulfate and hydroxyl radical based advanced oxidation of phenol. *Chem. Eng. J*. **224**, 10–16. (doi:10.1016/j.cej.2012.11.007)
66. Ding Y, Hu Y, Peng X, Xiao Y, Huang J. 2020 Micro-nano structured CoS: an efficient catalyst for peroxymonosulfate activation for removal of bisphenol A. *Sep. Purif. Technol*. **233**, 116022. (doi:10.1016/j.seppur.2019.116022)
67. Hammouda SB, Zhao F, Safaei Z, Srivastava V, Ramasamy DL, Iftekhar S, kalliola S, Sillanpää M. 2017 Degradation and mineralization of phenol in aqueous medium by heterogeneous monopersulfate activation on nanostructured cobalt based-perovskite catalysts $ACoO_3$ (A = La, Ba, Sr and Ce): characterization, kinetics and mechanism study. *Appl. Catal. B* **215**, 60–73. (doi:10.1016/j.apcatb.2017.05.051)
68. Mei Q, Sun J, Han D, Wei B, An Z, Wang X, Xie J, Zhan J, He M. 2019 Sulfate and hydroxyl radicals-initiated degradation reaction on phenolic contaminants in the aqueous phase: mechanisms, kinetics and toxicity assessment. *Chem. Eng. J*. **373**, 668–676. (doi:10.1016/j.cej.2019.05.095)
69. Devlin HR, Harris IJ. 1984 Mechanism of the oxidation of aqueous phenol with dissolved oxygen. *Ind. Eng. Chem. Fund*. **23**, 387–392. (doi:10.1021/i100016a002)
70. Babuponnusami A, Muthukumar K. 2012 Advanced oxidation of phenol: a comparison between Fenton, electro-Fenton, sono-electro-Fenton and photo-electro-Fenton processes. *Chem. Eng. J*. **183**, 1–9. (doi:10.1016/j.cej.2011.12.010)
71. Wu S, Zhao Y, Sun R, Sun Z, Yang C, Ma J. 2025 Chemistry, generation and regulation of reactive species in persulfate-based advanced oxidation processes. *Chem. Eng. J*. **515**, 163588. (doi:10.1016/j.cej.2025.163588)

72. Enguita FJ, Leitão AL. 2013 Hydroquinone: environmental pollution, toxicity, and microbial answers. *BioMed Res. Int*. **2013**, 542168. (doi:10.1155/2013/542168)
73. Chen H, Yao J, Wang F, Zhou Y, Chen K, Zhuang R, Choi MMF, Zaray G. 2010 Toxicity of three phenolic compounds and their mixtures on the gram-positive bacteria *Bacillus subtilis* in the aquatic environment. *Sci. Total Environ*. **408**, 1043–1049. (doi:10.1016/j.scitotenv.2009.11.051)
74. Duan L *et al*. 2023 General toxicity and genotoxicity studies of a new scale inhibitor for seawater desalination. *Environ. Sci. Eur*. **35**. (doi:10.1186/s12302-023-00722-7)
75. Khan A, Liao Z, Liu Y, Jawad A, Ifthikar J, Chen Z. 2017 Synergistic degradation of phenols using peroxymonosulfate activated by CuO-Co_3O_4@MnO_2 nanocatalyst. *J. Hazard. Mater*. **329**, 262–271. (doi:10.1016/j.jhazmat.2017.01.029)
76. Zeng H, Deng L, Yang K, Huang B, Zhang H, Shi Z, Zhang W. 2021 Degradation of sulfamethoxazole using peroxymonosulfate activated by self-sacrificed synthesized CoAl-LDH@CoFe-PBA nanosheet: reactive oxygen species generation routes at acidic and alkaline pH. *Sep. Purif. Technol*. **268**, 118654. (doi:10.1016/j.seppur.2021.118654)
77. Scaria J, Gopinath A, Nidheesh PV. 2021 A versatile strategy to eliminate emerging contaminants from the aqueous environment: heterogeneous Fenton process. *J. Clean. Prod*. **278**, 124014. (doi:10.1016/j.jclepro.2020.124014)
78. Pinchao G, Ortiz L, Galeano LA, Hidalgo A, Ramírez JH. 2021 Optimized CWPO oxidation of natural organic matter in continuous fixed bed reactor catalyzed by an extruded Al/Fe-PILC clay catalyst. *J. Environ. Chem. Eng*. **9**, 104634. (doi:10.1016/j.jece.2020.104634)
79. Hu P, Long M. 2016 Cobalt-catalyzed sulfate radical-based advanced oxidation: a review on heterogeneous catalysts and applications. *Appl. Catal. B* **181**, 103–117. (doi:10.1016/j.apcatb.2015.07.024)
80. Terhalle J, Kaiser P, Jütte M, Buss J, Yasar S, Marks R, Uhlmann H, Schmidt TC, Lutze HV. 2018 Chlorine dioxide-pollutant transformation and formation of hypochlorous acid as a secondary oxidant. *Environ. Sci. Technol*. **52**, 9964–9971. (doi:10.1021/acs.est.8b01099)
81. Ma J, Li H, Yang Y, Li X. 2018 Influence of water matrix species on persulfate oxidation of phenol: reaction kinetics and formation of undesired degradation byproducts. *Water Sci. Technol*. **2017**, 340–350. (doi:10.2166/wst.2018.147)
82. Liu S, Zhao X, Wang Y, Shao H, Qiao M, Wang Y, Zhao S. 2017 Peroxymonosulfate enhanced photoelectrocatalytic degradation of phenol activated by Co_3O_4 loaded carbon fiber cathode. *J. Catal.* **355**, 167–175. (doi:10.1016/j.jcat.2017.09.016)
83. Arifin MN, Jusoh R, Abdullah H, Ainirazali N, Setiabudi HD. 2023 Recent advances in advanced oxidation processes (AOPs) for the treatment of nitro- and alkyl-phenolic compounds. *Environ. Res*. **229**, 115936. (doi:10.1016/j.envres.2023.115936)
84. Ribeiro RS, Gallo J, Bañobre-López M, Silva AMT, Faria JL, Gomes HT. 2019 Enhanced performance of cobalt ferrite encapsulated in graphitic shell by means of AC magnetically activated catalytic wet peroxide oxidation of 4-nitrophenol. *Chem. Eng. J*. **376**, 120012. (doi:10.1016/j.cej.2018.09.173)
85. Jawad A, Lang J, Liao Z, Khan A, Ifthikar J, Lv Z, Long S, Chen Z, Chen Z. 2018 Activation of persulfate by CuOx@Co-LDH: a novel heterogeneous system for contaminant degradation with broad pH window and controlled leaching. *Chem. Eng. J*. **335**, 548–559. (doi:10.1016/j.cej.2017.10.097)
86. Cai C, Kang S, Xie X, Liao C, Duan X, Dionysiou DD. 2020 Efficient degradation of bisphenol A in water by heterogeneous activation of peroxymonosulfate using highly active cobalt ferrite nanoparticles. *J. Hazard. Mater*. **399**, 122979. (doi:10.1016/j.jhazmat.2020.122979)
87. Yang Q, Choi H, Al-Abed SR, Dionysiou DD. 2009 Iron–cobalt mixed oxide nanocatalysts: heterogeneous peroxymonosulfate activation, cobalt leaching, and ferromagnetic properties for environmental applications. *Appl. Catal. B* **88**, 462–469. (doi:10.1016/j.apcatb.2008.10.013)
88. Chowdhury M, Kapinga S, Cummings F, Fester V. 2019 Co_3O_4/TiO_2 hetero-structure for methyl orange dye degradation. *Water Sci. Technol*. **79**, 2018. (doi:10.2166/wst.2018.383)
89. Wang N *et al*. 2022 SnO_2 shells-induced rich Co2+ sites and oxygen vacancies in $Fe_xCo_{3-x}O_4$ nanocubes: enhanced peroxymonosulfate activation performance for water remediation. *Chem. Eng. J*. **439**, 135682. (doi:10.1016/j.cej.2022.135682)
90. Gao J, Qin T, Wacławek S, Duan X, Huang Y, Liu H, Dionysiou DD. 2023 The application of advanced oxidation processes (AOPs) to treat unconventional water for fit-for-purpose reuse. *Curr. Opin. Chem. Eng*. **42**, 100974. (doi:10.1016/j.coche.2023.100974)
91. Yusuf A, Giwa A, Eniola JO, Amusa HK, Bilad MR. 2022 Recent advances in catalytic sulfate radical-based approach for removal of emerging contaminants. *J. Hazard. Mater. Adv*. **7**, 100108. (doi:10.1016/j.hazadv.2022.100108)
92. Mahbub P, Duke M. 2023 Scalability of advanced oxidation processes (AOPs) in industrial applications: a review. *J. Environ. Manag*. **345**, 118861. (doi:10.1016/j.jenvman.2023.118861)
93. Honarmandrad Z, Sun X, Wang Z, Naushad M, Boczkaj G. 2023 Activated persulfate and peroxymonosulfate based advanced oxidation processes (AOPs) for antibiotics degradation – a review. *Water Resour. Ind*. **29**, 100194. (doi:10.1016/j.wri.2022.100194)
94. Tepud-Rodríguez JS, Cotazo-Mosquera OJ, Garcia-Mora AM, Hidalgo-Troya A, Galeano LA. 2026 Supplementary material from: Al/Co-pillaring of clays from concentrated precursors and catalytic performance in the phenol degradation by sulfate radicals. Figshare. (doi:10.6084/m9.figshare.c.8386439)